

# Bioinspired Materials: from Low to High Dimensional Structure

Ning Zhao,\* Zhen Wang, Chao Cai, Heng Shen, Feiyue Liang, Dong Wang, Chunyan Wang, Tang Zhu, Jing Guo, Yongxin Wang, Xiaofang Liu, Chunting Duan, Hao Wang, Yunzeng Mao, Xin Jia, Haixia Dong, Xiaoli Zhang, and Jian Xu\*

The surprising properties of biomaterials are the results of billions of years of evolution. Generally, biomaterials are assembled under mild conditions with very limited supply of constituents available for living organism, and their amazing properties largely result from the sophisticated hierarchical structures. Following the biomimetic principles to prepare manmade materials has drawn great research interests in materials science and engineering. In this review, we summarize the recent progress in fabricating bioinspired materials with the emphasis on mimicking the structure from one to three dimensions. Selected examples are described with a focus on the relationship between the structural characters and the corresponding functions. For one-dimensional materials, spider fibers, polar bear hair, multichannel plant roots and so on have been involved. Natural structure color and color shifting surfaces, and the antifouling, antireflective coatings of biomaterials are chosen as the typical examples of the two-dimensional biomimicking. The outstanding protection performance, and the stimuli responsive and self-healing functions of biomaterials based on the sophisticated hierarchical bulk structures are the emphases of the three-dimensional mimicking. Finally, a summary and outlook are given.

## 1. Introduction

After billions of years of evolution, nature has developed biomaterials with amazing properties or smart behaviors. These biomaterials are much admired by material scientists not only for their outstanding performances, but more importantly, for the fact that they are generally synthesized and processed in aqueous circumstance at room temperature with very limited supply of chemical resources available for living organism. The

Prof. N. Zhao, Z. Wang, C. Cai, H. Shen, F. Liang, D. Wang, C. Wang, T. Zhu, J. Guo, Y. Wang, X. Liu, C. Duan, H. Wang, Y. Mao, Dr. X. Jia, H. Dong, X. Zhang, Prof. J. Xu

Beijing National Laboratory for Molecular Sciences  
Laboratory of Polymer Physics and Chemistry

Institute of Chemistry

Chinese Academy of Sciences

Zhongguancun North First Street 2, Beijing 100190, China  
E-mail: zhaoning@iccas.ac.cn; jxu@iccas.ac.cn

DOI: 10.1002/adma.201401718



building blocks of biomaterials are always organized in sophisticated hierarchical structures, which are closely related with their functions. Preparation of manmade materials with the inspiration from nature has been one of the frontiers of materials science and engineering. Hundreds and thousands of papers on bioinspired materials have been published. The purpose of this review is to summarize the recent progress in the preparation of bioinspired functional materials from one to three dimensional levels. Selected examples are described with emphasis on the relationship between the structure and function.

In nature, there are numerous magical fibrous materials, such as the spider silk with the mechanical properties outperformed all the artificial fibers,<sup>[1–3]</sup> the polar bear hair with excellent thermal insulating and optical properties,<sup>[4,5]</sup> plant roots with multichannel structure,<sup>[6]</sup> the cactus spine with the function of directional fog collection<sup>[7]</sup> and so on. We classified these fibrous biomaterials as one dimensional (1D) materials and some biomimetic 1D materials mimicking the special structures or extraordinary functions of natural fibrous archetypes have been presented in section 2.

As an indispensable media between the bulk and exterior substances, interface or surface materials can be recognized as the most common two dimensional (2D) materials. Coatings, films and membranes are some usual examples of interface materials that we are familiar with. Nature shows us a more gorgeous picture of biological interfaces with surprising functions: superior wettability, structural color, antireflective property, reversible adhesion, low-drag and antifouling actions, which inspire scientists to fabricate artificial materials that mimic biological interfaces. Some recent reviews summarized the progress in the fabrication of bioinspired 2D materials mimicking the superhydrophobicity of lotus leaf,<sup>[8,9]</sup> structural color of butterfly,<sup>[10]</sup> dry and repeatable adhesion of gecko feet,<sup>[11]</sup> patterned hydrophilic-hydrophobic surface of desert beetle.<sup>[12]</sup> In section 3 of this review, we focused on the recent developments in 2D materials with color shifting, antifouling and antireflective functions. These functions are desirable for coatings used in special applications.

Natural and artificial materials often have to protect themselves from outer damage caused by quasi-static and dynamic mechanical loads. Biological composites such as bones,<sup>[13]</sup> nacres,<sup>[14,15]</sup> armors,<sup>[16,17]</sup> and pummelo peel<sup>[18]</sup> demonstrate outstanding protection performance via their sophisticated 3D hierarchical structure over a wide length scale ranging from nanometers to meters. The structures of these composites usually have some similar characteristics: the combination of hard and soft components and the complicated arrangement in multiscale. This design principle is valuable for the preparation of damping materials with wide applications in industry. Because of the special structure of bulk biomaterials, they also can be used as the raw materials to prepare artificial materials retaining the original structure characteristics. In section 4 of this review, we emphasized on the preparation of bioinspired damping materials with a gradient composition and/or microstructure, and fabrication of aerogels by using biomaterials as precursors was also involved. In addition, the smart behaviors of the biomaterials like stimuli response and self-healing were also mentioned. Finally, a summary and outlook were given.

## 2. Biomimetic One Dimensional Materials

### 2.1. Spider Silk

Spider silk has excellent mechanical properties outperforming all the artificial fibers. For example, the strength and modulus of the dragline silk can reach about  $4 \times 10^9 \text{ N m}^{-2}$  and 9.5–30 GPa, respectively, and the elongation of the flagellaform silk is more than 200%.<sup>[1,19]</sup> Scientists have revealed that two factors are vital: the nanoscale semicrystalline folding structure and the degree of hydration of the disordered fraction.<sup>[20]</sup> The  $\beta$ -sheet crystals interlock molecules together while the less organized ‘amorphous’ regions endow molecules mobility.<sup>[21]</sup>

Unlike silkworms, the territorial nature of spiders makes it difficult to raise spiders on a large scale. Many researchers have devoted themselves to studying the structure of the silk and the spinning process in order to achieve an extraordinary mechanical performance with high production. Major ampullate spidroin 1 (MaSp1) and major ampullate spidroin 2 (MaSp2) have been testified as two major components of spider dragline silk. By introducing bioengineering techniques, recombinant MaSp1/MaSp2 “silk” fibers were produced according to the MaSp1 and MaSp2 sequences in a single protein. Although the mechanical properties of the synthetic silk fibers underperformed the natural silks in all regards (the strength and modulus of nature silks are 100.2 MPa and 6.17 GPa, respectively), the research testified that altering protein motif composition could modify the mechanical properties.<sup>[22]</sup> Further, a technology including wet-spinning, fiber extrusion and a mechanical post-spin treatment was developed to fabricate silk fibers. It is the first report to achieve visual representation of step-by-step spin process and analyze artificial silk fibers on a laboratory scale.<sup>[23]</sup> Inspired by the unusual mechanical strength and the excellent biocompatibility and biodegradability of natural silk, Tsukruk group prepared some porous silk microcapsules with controlled permeability. The silk microcapsules fabricated by “silk-on-silk” LbL technique



**Prof. Ning Zhao** is an associate professor at the laboratory of polymer physics and chemistry of the Institute of Chemistry, Chinese Academy of Sciences (ICCAS). He received his B.S. (2000) and M.S. (2003) degrees from Tianjin University, China, and Ph. D. from ICCAS in 2006. After that he did a postdoctoral research at the University of Montreal (2007–2008). His research interest includes biomimetic materials, surface modification.



**Prof. Jian Xu** was graduated from Sichuan University in China, where he got his B.S. and M.S. in 1982 and 1985, respectively. After working at the Beijing University of Chemical Technology for seven years, he returned to Sichuan University and got his Ph. D. in 1994. He was a postdoctor from 1995 to 1997 at ICCAS, and then was a visiting researcher from 1998 to 1999 at Hokkaido University. He is now a full professor at ICCAS. His main research areas are smart gels, biomimetic materials, high technology fibers.

own outstanding mechanical properties as the silk protein random coils formed a  $\beta$ -sheet-rich structure by treatment with methanol in the fabricating process.<sup>[24]</sup> The silk ionomer microcapsules made from silk fibroin counterparts modified with poly(lysine) and poly(glutamic) acid were also extremely robust due to the strong interactions of ionic pairing and covalent cross-linking. In addition, their controlled permeability is owing to the reversible swelling/deswelling response triggered by different pH values.<sup>[25]</sup>

Apart from the classical mechanical properties, the spider native dragline silk has the ability to undergo super-contraction when it contacts with water or in a relative humidity higher than 60%. This is because the reorientation of hydrogen bonds between the spider silk protein molecules during the process of water uptake.<sup>[21,26]</sup> In addition, by the method of non-invasive light scattering, Qin et al. revealed that the super-contraction could not only increase the stiffness by more than 40%, but shorten the signal transfer time by more than 20%, thus increasing the sensitivity of the spider for the location of the prey.<sup>[27]</sup> Agnarsson and colleagues used dry and wet air to control the contraction and relaxation of spider silk to act as a high performance biological muscles. The power density of the silk based muscles is 50 times higher than other biological muscles (Figure 1a).<sup>[21]</sup>

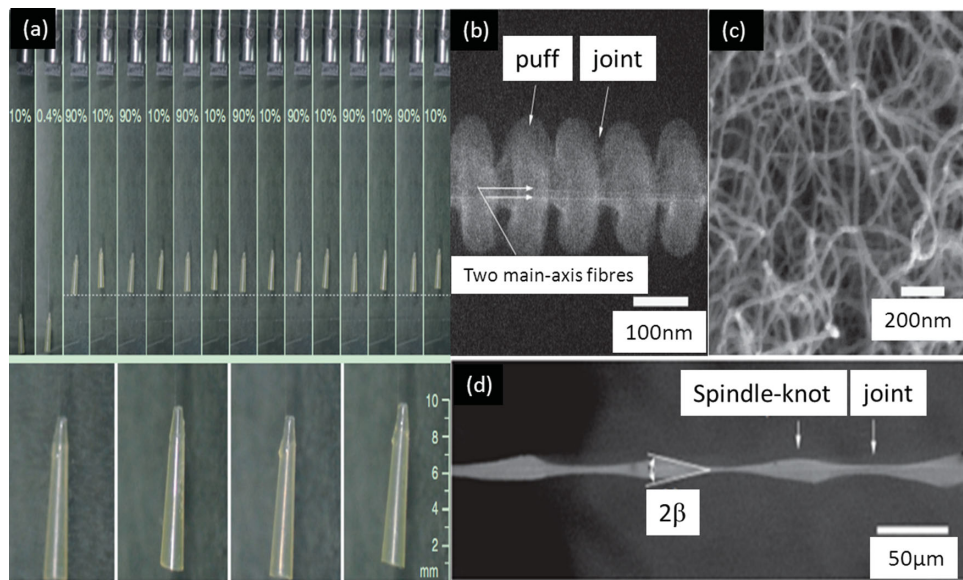


**Figure 1.** (a) Snapshots showing the lifting performed by spider dragline silk during repeated cycles of wetting and drying. The single 5.5  $\mu\text{m}$  diameter silk thread repeatedly lifted the 9.5 mg weight through seven cycles of drying (top). The average displacement during each contraction was 0.65 mm or 1.7% of the thread's total post-supercontraction length (bottom). Reproduced with permission.<sup>[21]</sup> Copyright 2009, Company of Biologists. (b) Low magnification environmental SEM image of dry capture silk: periodic puffs and joints, (c) Magnified SEM image of spindle puffs covered with random nanofibrils, and (d) Environmental SEM images of wet capture silk: spindle-knots linked by joints. Reproduced with permission.<sup>[28]</sup> Copyright 2010, Nature Publishing Group.

Except for the remarkable mechanical properties and supercontraction, the capture silk can also directionally collect water from humid air. *Uloborus walckenaerius*, one of the cibellate spiders, whose dry capture silk is consisted of periodic puffs composed of countless nanofibrils and joints (Figure 1b,c). When the spider silk is in mist, a few tiny water drops first condense on the puffs, and then the “wet-rebuilt” process will happen: puffs shrink to opaque bumps to form spindle-knots with water condensing. Consequently, the wet-rebuilt spider silk consists of spindle-knots covered with random nanofibrils and joints with nanofibrils aligned relatively parallel to the silk axis (Figure 1d).<sup>[28]</sup>

Two driving forces contributing to the directional water collection were presented: the Laplace pressure difference as the radius of the spindle-knot is larger than that of the joint, and the surface energy difference as the roughness of the joint is larger than that of the spindle-knot. Several biomimetic fibers with the function of directional water collection were fabricated. Jiang et al. dipped nylon fiber in a polymer solution firstly and then drew the fiber out horizontally at a certain velocity. A cylindrical polymer film was formed on the fiber surface at the beginning and then spontaneously broke up into droplets along the fiber owing to the Rayleigh instability, leading to the formation of the bead-in-string structure. By introducing non-solvent in polymer solution, porous nanostructure on the spindle-knots was obtained by phase separation. In this method, the surface tension and viscosity of the polymer solution and the fiber drawing velocity were revealed crucial to achieve the spider silk-like fiber, and the moving direction of tiny water (“toward” or “away from” the knot) could be controlled by optimizing the curvature, chemical and roughness gradients on the fiber surfaces.<sup>[29]</sup> Further, a fluid-coating method to continuously

fabricate inexpensive and durable bioinspired fibers on a large scale were presented.<sup>[30]</sup> In addition, the electrodynamic and microfluidic technologies were introduced to get the spider silk-like fibers.<sup>[31]</sup>

Up to date, there are still numerous structures and functions about spider silk unexploited. The focuses of the biomimicry about spider silk are on the mechanical properties of high strength, extensibility and super-contraction, and the water directionally collection. Much more functions of spider silk may be expected in future.

## 2.2. Polar Bear Hairs

The polar bear hairs are hollow in structure along their length and nearly transparent containing no pigmentation. Besides, the hollow hairs have a smooth external surface but a rough core (Figure 2a). Air can be captured not only in the hollow structure of each hair, but also among the hairs, which allows the heat radiation go through, but the convection and conduction of the heat are impeded. This special structure plays an important role in thermal insulating and keeping warm. In addition, the polar bear hairs can also guide light transmission like optical fibers and trap light especially the ultraviolet radiation.<sup>[4,5]</sup>

Inspired by the structures and functions of polar bear hairs, Bahners et al. used wave-guiding polymer poly(methyl methacrylate) (PMMA) as the core fiber, and coated the core fiber with fluorescent dyes dispersed in a methanol solution of 5% poly(vinyl acetate) (PVA). The optical effect could be achieved well. But that effect is significantly reduced when PMMA is replaced by poly(ethylene terephthalate) (PET) because of the

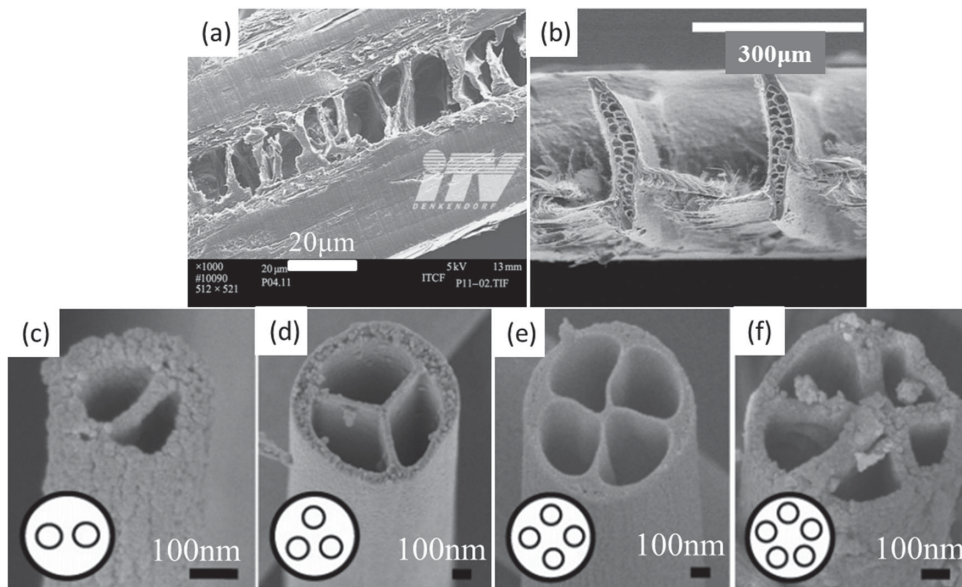


**Figure 2.** (a) SEM image of polar bear hair. Reproduced with permission.<sup>[32]</sup> Copyright 2009, Royal Society of Chemistry. (b) Transverse section of rami of remex of *Nothoprocera perdicaria*. Reproduced with permission.<sup>[37]</sup> Copyright 2013, Elsevier. (c-f) SEM images of multichannel tubes with variable diameter and channel number. Reproduced with permission.<sup>[33]</sup> Copyright 2007, American Chemical Society.

pronounced scattering and attenuation in this semi-crystalline fiber.<sup>[4]</sup> What is more, the light-conductive and stable polymer fibers can be used into solar collector system. Stegmaier et al. developed a new flexible and mobile solar collector system by coating transparent silicone rubber on the translucent polymer fibers. Owing to the specific structures and chemical compositions, the emission of long-wave radiation can be prevented and the convection is reduced.<sup>[32]</sup>

To mimic the hollow structure of polar bear hair, TiO<sub>2</sub>/PVP hollow fibers were fabricated by coaxial electrospinning.<sup>[6]</sup> Further, to mimic the multichannel structure of lotus root, the fiber with multichannel structures were prepared by coaxial electrospinning using 20% poly(vinyl pyrrolidone) (PVP) ethanol solution as the outer liquid, and paraffin oil as the inner liquid. These multichannel fibers may have potential applications in lightweight and thermo-insulated textiles, high efficiency catalysis and multi-component drug delivery (Figure 2c-f).<sup>[33]</sup> Although coaxial electrospinning is an effective and versatile method to fabricate hollow fibers of various materials, Xu et al. also prepared porous hollow CuO nanofibers by single-spinneret electrospinning of PVP/copper acetate homogeneous precursor solution followed by annealing and reduction.<sup>[34]</sup>

Due to the various functions based on the hollow fiber structure, using the natural hollow fiber as template is a straightforward method to prepare engineering hollow fibers. Similar to polar bear hairs, kapok fiber, a natural plant fiber, also has a hollow structure. Hollow carbon fibers were obtained by using natural kapok fiber as the template and followed by sintering at higher temperature.<sup>[35]</sup> Besides the traditional application of kapok fibers as absorbents and buoyancy materials, Xu et al. found that the hollow structure has an excellent acoustic damping property and shows a promising application as sound adsorption materials.<sup>[36]</sup>

### 2.3. Additional Examples

Cactus spine is a good archetype in nature to mimic. Ju et al. found that the subtle architectures of the spine, namely the oriented barbs on the tip, the gradient grooves in the middle and the belt-structured trichomes at the base, endowed the cactus fantastic fog collection property.<sup>[38]</sup> The driving forces are considered to be the gradient of the Laplace pressure caused by the conical shape, the gradient of the surface tension caused by the surface roughness, and the anisotropy of the contact angle hysteresis caused by the aligned grooves. Although cactus has been investigated for a long time, the study of biomimetic materials inspired by cactus just begins. Recently, the Cu based cactus spine-like needles were prepared by an electroetching method and the PDMS based cactus spine-like needles were prepared by a template method. These above oleophilic spine-like conical needle arrays can be used for the continuous collection of micron-sized oil droplets from water.<sup>[39]</sup>

In nature, there are many branched hollow fibers, such as capillaries in the blood vessel system and the feathers of many birds (Figure 2b).<sup>[37]</sup> The branched hollow structure usually has a series of functions, such as weight reduction, air or liquid transportation, thermal insulating and so on. Mimicking this unique structure is of much importance for engineering fibers. Qiu et al. discovered that self-assembled fibrous structure can be formed after a relative long-term aging of PVP solution under room temperature. Based on this phenomenon, they successfully fabricated hollow branched silica and gold fibers by using PVP as the template. Their work also suggested that this method could be universal for directing the formation of branched hollow inorganic fibers.<sup>[40]</sup>

By mimicking the silicification in nature, mesoporous silica helical fibers were synthesized using a catanionic-neutral ternary surfactant (CnTMAB-SDS-P123 ( $n = 14-18$ )) in a highly

dilute silica solution.<sup>[41]</sup> The yield of the surfactant-templated helical fibers was revealed to be dependent on water content, reaction temperature and pH value of the solution. This mesoporous silica helical fiber can be used as a solid template to prepare other mesoporous helical fibers, such as carbon helical fibers.

The biomimetic 1D materials have been studied for a long time, and numerous 1D materials in nature with special structures and functions have been found. Some natural biomimetic archetypes have already been studied deeply and widely, however, there are still a lot of work to be done. For examples, current research on spider silk covers the gene composite, the protein structure, the spinning process, the mechanical properties and the function of directional fog collection. However, when taking into account the diversity of spider species, there are still many unknown nice properties to be exploited. The study of the polar bear hairs and the bamboo fiber has a long history, but the research is limited in a few fields, like the thermal insulating materials and the fiber reinforcement composites. The cactus spine, as a new biomimetic archetype, opens up a new direction for learning from nature, but the related work just begun.

The introduction of the concept of biomimicry may promote the cooperation of some interdisciplines, such as zoology, botany, chemistry, physics, engineering and so on, which will promote the development of the biomimetic materials. So far, the focuses of the biomimetic 1D materials are mainly on the structure and a few functions, but lacks the building of the models and abundant theoretical research. Furthermore, the applications of the biomimetic 1D materials have been prevented by the immature equipment and technology, the poor durability and the unavailable large scale production of the prepared biomimetic materials. Thus, the improved equipment and technology, optimized fabricating method, the integration of multifunction may be the trends of the biomimetic 1D materials. Certainly, looking for some new biomimetic archetypes with particular functions is also an encouraging work.

### 3. Bio-inspired Two Dimensional Materials

#### 3.1. Electrochromic Color Shifting Coatings

After the development for hundreds of million years, nature has evolved into a huge art gallery of beautiful colors. Three main sources including pigments, structural coloration and bioluminescence, make up the polychrome of nature. Among them, structural coloration has caught more scientific attention recently. Different from others, the dazzling and bright structural colors displayed in animals and plants are mainly resulted from ordered micro/nanostructures.<sup>[42]</sup>

For examples, Saranathan et al. found out that biophotonic nanostructures of *Callophrys* butterfly wings form vivid structural colors.<sup>[43]</sup> In addition, the dazzling colors presented by other butterflies were believed to come from the micro/nanostructures on their wings as well.<sup>[44–47]</sup> Structural colors also exist on the feathers of certain birds. The blue coloration of scarlet macaw feather does not change with perspective angle, showing a noniridescent characteristic. The bright blue color is

brought by an amorphous diamond-structured photonic crystals with only short-range order.<sup>[48]</sup> For years, structural coloration has been observed and studied mostly in animals, while some prominent examples of the iridescent coloration from plants have also been presented. The periodic striated epidermis on the flowers of *Tulip* "Queen of the night",<sup>[49]</sup> the four lamellae in the upper cuticle of the leaves of *Selaginella willdenowii*,<sup>[50]</sup> and the helicoidal structures of the fruits of *Pollia condensata*<sup>[51]</sup> contribute to the observed iridescent colors, respectively.

Other than structural colors, there is another special phenomenon in nature that some insects can control and tune their body color for camouflage, hiding them from the attack of their enemy or attract prey. The wings of *Closterocerus coffeeellae* can display different color patterns depending on the background.<sup>[52]</sup> The crab spiders of the family *Thomisidae* are able to change their body color reversibly from white to yellow, within several days.<sup>[53]</sup> *O. Ceratophthalmus* juveniles are exceptionally well camouflaged to the beach substrate.<sup>[54]</sup>

In an electrochromic system, the electroactive materials can change the light absorption properties in visible, infrared or even microwave region via redox reaction stimulated by low direct current potential, resulting in a reversible color shift. The first polymer electrochromism device was reported by Burroughes in 1989.<sup>[55]</sup> Over the last couple of decades, electrochromism device (ECD) based on conducting polymers has been paid much attention by the researchers, and a variety of ECDs with multicolour, flexible substrate, and patterning have been reported.

Invernale and his colleagues processed an assembled soluble thiophene derivative into solid-state device, which could switch from the yellow precursor (up) to the red (bottom) neutral state and back to blue (middle), irreversibly (Figure 3a).<sup>[56]</sup> Shin et al. used electrochromic polymers with different colors (red, blue, green, and yellow) to complete a complementary ECD. This ECD was placed above a paper printed with a black and white bouquet and could switch between transparent yellow and black color. It is noteworthy that various color tones of RGBY can be obtained at potentials between  $\pm 2V$ , suggesting this ECD can camouflage to black surrounding in color at the oxidized state (Figure 3b).<sup>[57]</sup> Another patterned ECD was prepared by Kim et al., in which thiophene derivatives with photo functional group were used as electrochromic layer. Figure 3c shows the color change of the patterned ECD, even on a flexible substrate.<sup>[58]</sup> Reynolds group<sup>[59,60]</sup> reported how to obtain electrochromic polymer solutions with full color palette. They designed electrochromic patterns: a tree and a butterfly (Figure 3d,e), by spray coating the ECP solutions through a shadow mask applied to the conductive substrates. Using the method, it is convenient to manufacture ECD with various patterns.

Metal oxides are another important kind of electrochromic materials. For example, Chen<sup>[61]</sup> and Costa<sup>[62]</sup> prepared  $WO_3$ -based ECD on ITO glass and flexible PET, respectively. Another innovative ECD based on silver nano particles exhibiting a change in color between black, mirror, red and blue, was demonstrated by the group of Kobayashi.<sup>[63,64]</sup>

Adaptive camouflage and chameleonic systems have aroused great interest in the past and more underlying and cooperative technologies are still required for the further development.<sup>[65]</sup> For this, more ingenious design in ECD structure and wider

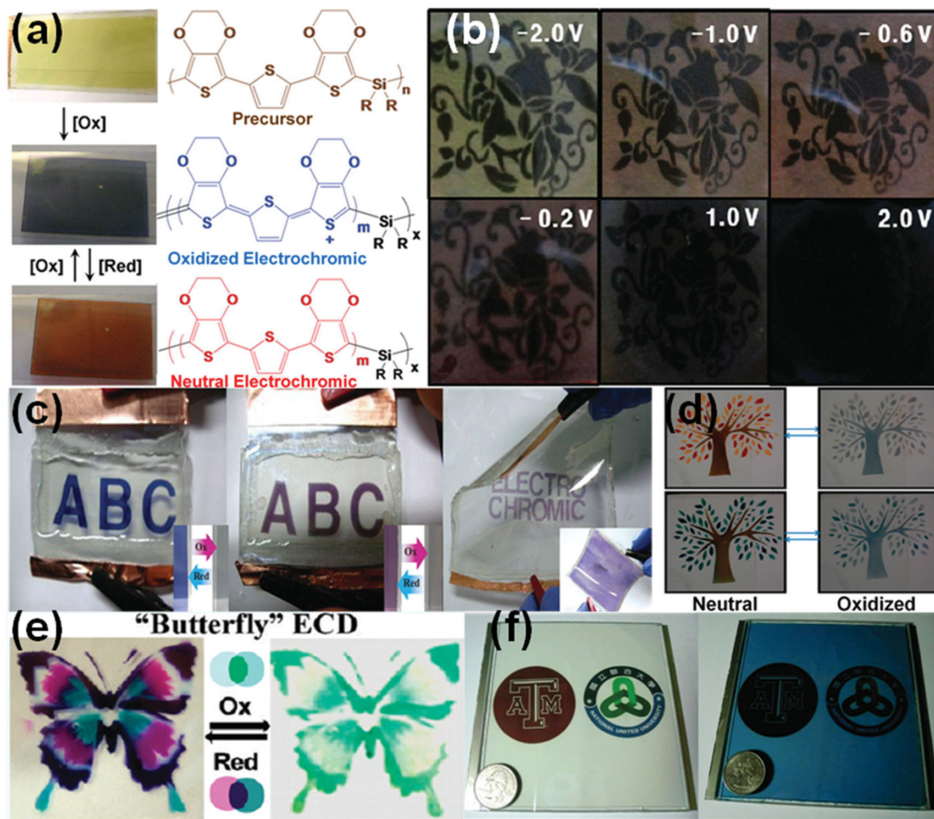


**Figure 3.** A variety of ECDs with multicolour, flexible substrate and patterning. (a) Photographs of the solid-state device based on thiophene derivatives, (top) the assembled yellow precursor device, (middle) the blue oxidized state and (bottom) the red neutral state.<sup>[56]</sup> (b) Photographs of electrochromic device at different potentials, taken after placing it on a white paper background with black bouquet. Reproduced with permission.<sup>[57]</sup> Copyright 2012, American Chemical Society. (c) Window typed patterned electrochromic devices: (Left) PEDOT-MA, (Centre) PProDOT-MA (insets show the color states attained in each configuration) and (Right) Flexible ECDs using PProDOT-MA on ITO films (inset shows a same sized flexible ECD without patterning process).<sup>[58]</sup> (d) Patterned films of various polymers created by spray-casting through a shadow mask on ITO/glass electrodes. Reproduced with permission.<sup>[59]</sup> Copyright 2011, American Chemical Society. (e) Photographs of a multicolored window ECD on In<sub>2</sub>O<sub>3</sub>/Ag/Au-coated PET electrodes (with an active area of 2.7\*1.7 in.). The ECD was switched from neutral (left) to oxidized state (right). Reproduced with permission.<sup>[60]</sup> Copyright 2011, American Chemical Society. (f) Images of WO<sub>3</sub>-based ECD on ITO glass in a bleached state (Left) and colored state (Right), respectively.<sup>[61]</sup>

selection in electrode materials are needed besides the preparation of electrochromic materials.

### 3.2. Color Shifting Photonic Crystals

It is efficient to adjust the structural coloration by modulating the refractive index and periodic structure of the photonic crystal.<sup>[66]</sup> More specifically, the photonic crystals can change their colors and show up in different colors, and even achieve full-color when they are subjected to a changing outer surroundings or under various stimuli, such as electricity, chemicals, humidity, temperature, external force and so on.

Color-changing polyelectrolyte gel was reported by Ueno.<sup>[67]</sup> Under the electric field, the inverse opal polyelectrolyte gel was irritated by electro dragging force, thus altering the lattice constant along the thickness direction and triggering a reversible transformation from green to blue. Highly charged silica-coated ZnS colloids were synthesized by researchers from Samsung Electronics. The colloids could self-assemble into long range

ordered photonic crystal owing to a powerful electrostatic repulsion between the particles. As shown in Figure 4a, red, green, and blue colors were observed by tuning the stopband via increasing the potential.<sup>[68]</sup>

Chemically responsive photonic crystals are complicated systems, because of the influences of various chemical environments, covering pH, ionic strength, solvent and vapor molecules, biomolecules and so forth. Asher et al.<sup>[69]</sup> developed a 2D photonic crystal sensor with high diffraction efficiency for ionic and pH sensing application. Liu et al.<sup>[70]</sup> reported another fast and simple naked eye detector using a TiO<sub>2</sub> inverse opal penetrated by PANI, which could change the color in NH<sub>3</sub> and HCl vapors (Figure 4b). Zhang et al.<sup>[71]</sup> prepared a bioinspired hierarchically structured photonic crystals detector by incorporating polymethylacrylic acid into a *Morpho* butterfly wing through a surface bonding and polymerization route. This sensor showed color change from blue to green when pH decreased from 10.51 to 1.62. Furthermore, a simple solvent and anion sensor, made of inverse opal hydrogels formed by crosslinking DMC-co-MMA copolymer using well-ordered 3D silica opal as

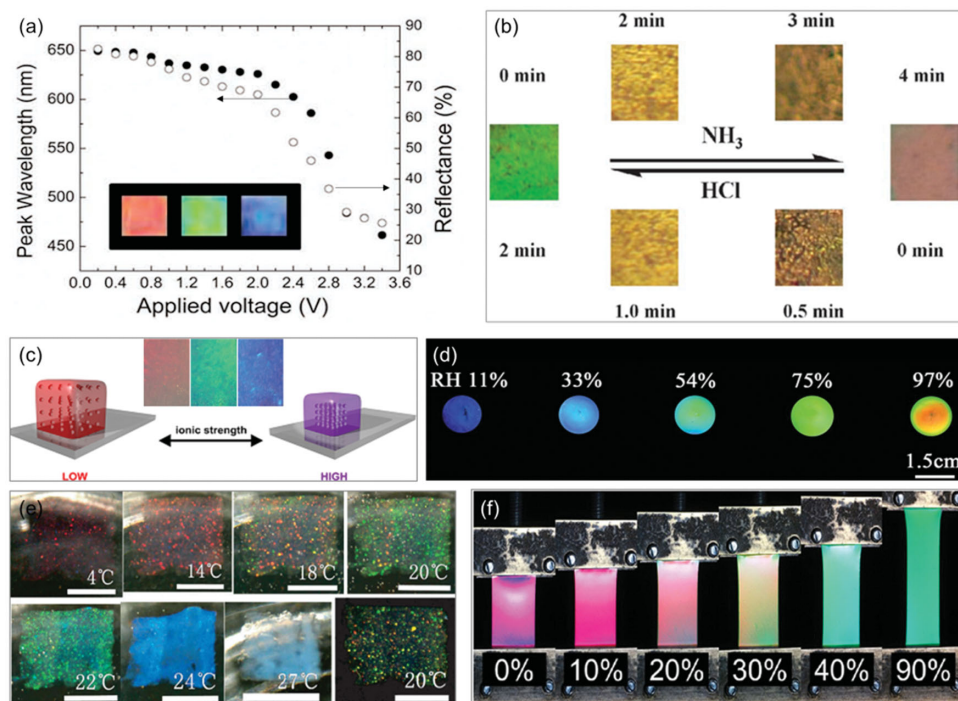


**Figure 4.** Color shifting of photonic crystals. (a) Relationship between applied voltage *vs.* reflectance and peak position of photonic crystals films.<sup>[68]</sup> (b) Photographs of the as-constructed photonic Crystals corresponding to different exposure times to NH<sub>3</sub> and HCl vapor.<sup>[70]</sup> (c) The schematic for the color shifting of a sensor layer composed of a polyacrylamide hydrogel matrix containing colloidal photonic crystals. The inset shows the color changes of this sensor layer: red in pure water; green in a sodium chloride solution ( $10^{-3}$  mol L<sup>-1</sup>); purple at  $c(\text{NaCl}) = 10^{-1}$  mol L<sup>-1</sup>. Reproduced with permission.<sup>[73]</sup> Copyright 2013, American Chemical Society. (d) Digital photos of the photonic humidity sensor in different humidity environments, showing color changes from navy blue to light red. Reproduced with permission.<sup>[79]</sup> Copyright 2012, Royal Society of Chemistry. (e) Photographs of a freestanding PMCC film taken when temperature rising from 4 to 27 °C. The last one (bottom right) was taken when the film was cooled back to 20 °C. The film was immersed in 0.5M NaCl solution, pH 3.0. Scale bar: 0.5 cm.<sup>[81]</sup> (f) Reflection colors of the elastomeric opal film under strains up to 90%. Reproduced with permission.<sup>[83]</sup> Copyright 2013, American Chemical Society.

template, was also obtained.<sup>[72]</sup> Upon soaking in heterogeneous anion solutions, the sensor was able to exchange with anions in the solution to shift the color, only when the hydrogels became wetting. It is worth mentioning that the solvent and anion response could be captured as independent, realizing the detection of two stimuli simultaneously. Fenzl et al.<sup>[73]</sup> also presented an ionic detector of polyacrylamide hydrogel using cross-linked polystyrene nanoparticles as temple. The film shows red color when placed in fresh water, but turns to green in a 1mM electrolyte solution such as sodium chloride, and to purple in the presence of 100mM electrolyte solution (Figure 4c). Huang et al.<sup>[74]</sup> fabricated a microchip containing multi-stopband photonic crystals for high performance metal-ion recognition, which can identify and analyze 12 different metal ions.

Beyond that, photonic crystals can also be used as sensors to detect saccharides. A novel dual signal glucose reporter with an inverse opal structure was developed by Jin.<sup>[75]</sup> The catalytic product of enzyme-catalytic redox reaction for glucose caused the change in the microenvironment, which induced shrinkage of the hydrogel and a corresponding blue shift of the reflection peak. The color change also can be visibly observed by the naked eyes. Ayyub et al.<sup>[76]</sup> investigated a photonic crystal film as a sensitive and selective fructose sensor, fabricated from a self-assembled lamellar block copolymer. When immersed into a 50mM fructose solution, the film exhibited a noticeable color

change from blue to orange. In the presence of glucose, mannose and sucrose, this film is able to selectively recognize and respond to fructose.

Hawkeye et al.<sup>[77]</sup> took advantage of glancing angle deposition technique to prepare a mesoporous TiO<sub>2</sub> photonic crystal, which exhibits obvious color-shift in response to small changes in humidity. Zulian et al.<sup>[78]</sup> prepared core-shell colloids by surfactant free emulsion radical copolymerization of hydrophobic styrene and hydrophilic methacrylic acid. The self-assemble opal film shows a color change at different humidity and pH values. Hu et al.<sup>[79]</sup> introduced a quick and convenient way to manufacture a humidity sensor on a large scale with arbitrary shapes. Carbon encapsulated superparamagnetic microspheres were spontaneously assembled under magnetic field, followed by an instant radical polymerization to fix the photonic crystal structures inside a polyacrylamide glycol gel matrix. Figure 4d shows the digital photo of the gel sensor in different humidity environments, changing its color from navy blue to light red. By using the phase-separation method, Kumano et al.<sup>[80]</sup> demonstrated a porous gel exhibiting angle independent structured color and reversible color change depending on the composition of the mixed solvent in the gels as well as the environmental temperature.

In addition, several photonic crystals in hydrogel can change its colors in response to temperature. Chen et al.<sup>[81]</sup> prepared

soft PNIPAM microgels which can self-assemble into colloidal crystals with high order. Figure 4e shows the photographs and diffraction spectra of the freestanding microgel film. It is highly swollen and red color at 1 °C, and shrinks gradually upon heating, simultaneously with color shifts gradually to green, blue, and finally white. Matsubara et al.<sup>[82]</sup> introduced porosity into a gel by using colloidal crystal as template and the structural color of the porous gel turned from dark red to yellow, to green, finally, generated blue as the temperature increased.

Compared with stimulus condition involving temperature, humidity and chemicals, mechanical pressing or stretching represents a conceptually straightforward but effective mode to control the photonic crystal structures and change their color. Schäfer et al.<sup>[83]</sup> reported a new strategy to achieve mechanical responsive elastomeric polymer opal films. Takeing advantage of semicontinuous emulsion polymerization, the novel monodispersed highly functional core-interlayer-shell beads are obtained, with a temperature-sensitive fluorescent rhodamine dye located either in the core or the shell. The opal film shows fascinating stretch-tunable properties. As demonstrated in Figure 4f strains of only a few percent already caused a blue shift of the reflected color. Fudouzi et al.<sup>[84]</sup> also demonstrated a PDMS rubber sheet whose gradients in color were observed from red to yellow-green due to mechanical strain. These stretching responsive materials can be employed in practical applications such as mechanical sensing, strain imaging, and smart sensing.

Beyond that, some thin-film materials based on photonic crystals exhibit many functions under various stimuli. Yue et al.<sup>[85]</sup> synthesized a high toughness lamellar hydrogel, showing ternary stimuli-responsive structural color changes. The gel consisted of alternating hard and soft layers of polymeric surfactant and interpenetrating poly(acrylamide)-poly(acrylic acid) networks, respectively. Wide range switching of the stop-band position can be realized due to the stimuli of temperature pH and stress/strain.

In this part, an exciting field of color shifting photonic crystals with grand challenges is presented. In most cases, the color shifting photonic crystals are fabricated by self-assembly approaches, which have the advantages of lower costs and higher production efficiencies. However, the transition from laboratory investigation to commercial production requires large-scale manufacturing of these photonic structures in a highly efficient, consistent and reproducible manner. To improve the applicability of color-change systems, more attentions must be paid on the increase of the durability and the large scale production.

### 3.3. Bio-inspired Antifouling Surfaces

Surfaces immersed in seawater are easily subjected to varieties of marine organisms (bacteria, diatoms, algae, barnacles and other invertebrates), causing the so-called marine biofouling.<sup>[86,87]</sup> The occurrence of marine biofouling has several devastating impacts, for example, increase of surface roughness of the hull and consequently the oil consumption, acceleration of coating deterioration and increase of the frequency of dry-docking operations.<sup>[88]</sup> Strategies for preventing marine

biofouling have been developed for a long time. By far, the most effective and low-cost solution was self-polishing tributyltin (TBT) coatings, however, it has been completely banned by IMO treaty since 2008 because of the adversely effect of TBT to the growth of oysters and some other untargeted organisms.<sup>[89,90]</sup> Since the end of last century, numerous designs and developments for environment-friendly antifouling (AF) technology have been explored.<sup>[91]</sup> Among them, biomimetic solutions may be the most promising ones, given that many natural surfaces in the sea exhibit perfect AF properties and moreover these natural solutions are absolutely friendly to the marine environment and ecosystem.

Many marine creatures including marine mammals, echinoderms, algae, mollusks and crustaceans have been investigated, with an in-depth understanding of the mechanisms behind natural AF performances. The corresponding progresses have been summarized elsewhere.<sup>[92]</sup> Nevertheless, marine biofouling is very complex since the marine organisms cover a wide range of creatures from protozoa to algae and mollusk. It is difficult to control biofouling just through one single means.

Stokes and his co-workers summed up all possible factors that might influence natural AF performances, both intrinsic and extrinsic ones. The factors were defined as 1) surface physical features, 2) topography, 3) textures, 4) mechanical, 5) wall shear stress, 6) natural chemical defenses, 7) biological signals. Ralston and Swain<sup>[93]</sup> tried to generalize the mechanisms in a more brief way as physical, chemical, mechanical and behavioral. Most of the bio-inspired attempts of fabricating AF surfaces encompassed these principles.

#### 3.3.1. Surface Roughness

The implication of surface roughness or topography on the settlement of fouling organisms has been emphasized in many reports, where several biomimetic models (as shown in Figure 5) are investigated.<sup>[94–99]</sup> Many fast swimming fishes or marine mammals are believed to be non-fouling as a result of the special physical properties of their skins.

As a typical model, the skin of shark has been investigated profoundly. The regularly arranged ridged platelet structures of shark skin have inspired the commercial product named Sharklet.<sup>[100]</sup> As an AF strategy, Sharklet textures were fabricated on PDMS substrate through photolithography.<sup>[100,101]</sup> AF performances of various patterns with different feature sizes were examined and it had been found feature size is the key factor in the repellent of fouling organisms. Settlers with bigger size than the feature size of the surfaces are unlikely to settle on the substrates. On the basis of this theory, Efimenko et al. examined AF properties of a series of complex, hierarchically wrinkled surfaces, expecting the hierarchical feature sizes would make a broad-spectrum resistance of biofouling (Figure 6a).<sup>[102]</sup> Field tests showed a successful free-fouling for over a year, indicating the effectiveness of this scenario. Pilot whale skin is another instance of engineered surface. In the case of *Globicephala Melas*, the surface of the skin is covered with nano-ridge pores, which contribute to the non-fouling property.<sup>[94,103,104]</sup> Inspired by the whale skin, researchers utilized multi-layered polyelectrolytes to produce a range of nano- and micro-structured

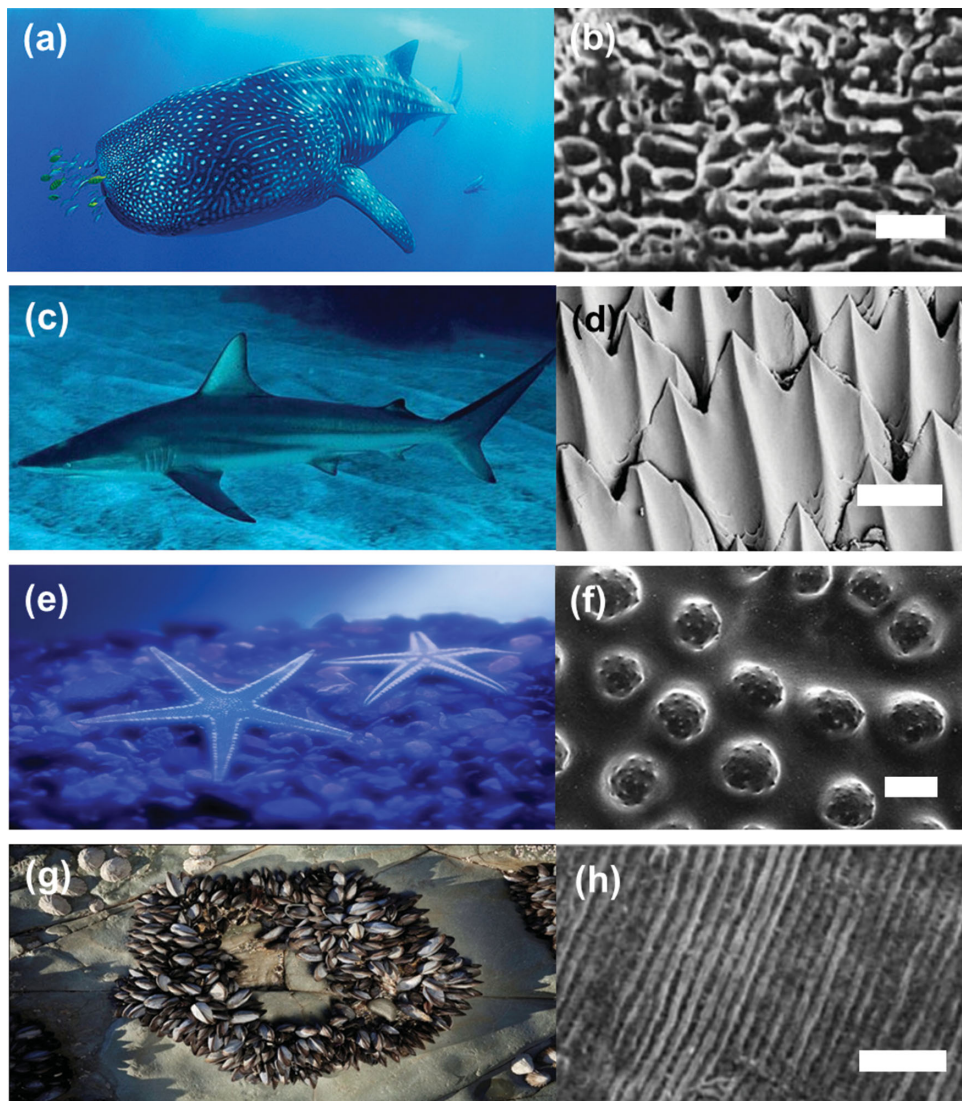


**Figure 5.** Several natural antifouling models and their corresponding surface microstructures. (a, b) Pilot whale. Reproduced with permission.<sup>[94]</sup> Copyright 2002, Springer. (c, d) Shark, (e, f) sea stars. Reproduced with permission.<sup>[98]</sup> Copyright 2007, Springer. (g, h) Mussels. Reproduced with permission.<sup>[99]</sup> Copyright 2003, Springer. The scale bars in (b, d, f and g) are 1 µm, 100 µm, 100 µm and 10 µm, respectively.

surfaces, which showed feature-size dependent AF performance regardless of surface chemistry (Figure 6b).<sup>[105]</sup> Other models like dogfish egg-case, molluscs, echinoderms and so forth, were elaborated elsewhere.<sup>[87,91]</sup>

In addition to the fabrication of biomimetic engineered textures, nowadays, research efforts have been devoted to explain the relationship between attachment behavior and surface roughness, which will provide better understanding of the mechanism and guide the design of structured AF coatings. Reduction of attachment points or adhesive contact area is believed to be a crucial factor in this mechanism. Algorithm and models<sup>[104,107,108]</sup> were built to describe the correlation between the attachment density of fouling organisms and surface structural features. Additionally, hydrodynamic variations introduced by structured surfaces in dynamic conditions were considered as another possible principle to deter attachment of the fouling organisms.<sup>[106,109]</sup>

### 3.3.2. Wettability

Many efforts have been focused on the connections between self-cleaning and AF property, but it remains elusive. Genzer et al.<sup>[110]</sup> presented a synopsis of implications of superhydrophobicity on marine biofouling, demonstrating wettability might play a part in AF performance to some degree, but was not omnipotent when faced with the diverse fouling organisms. In fact, studies have shown that PEG modified hydrophilic surfaces strongly repel protein adsorption, whereas hydrophobic surfaces with low surface energy ( $20\text{--}30 \text{ mN}\cdot\text{m}^{-1}$ ) exhibit good resistance to macrofoulers.<sup>[86,91,111]</sup> Therefore, emphasis has been made on molecular designing and combination of both hydrophilicity and hydrophobicity.<sup>[111]</sup> PEGylated polymers, PDMS, fluoropolymers and amphiphilic polymers have been developed as alternatives of traditional matrix resins.

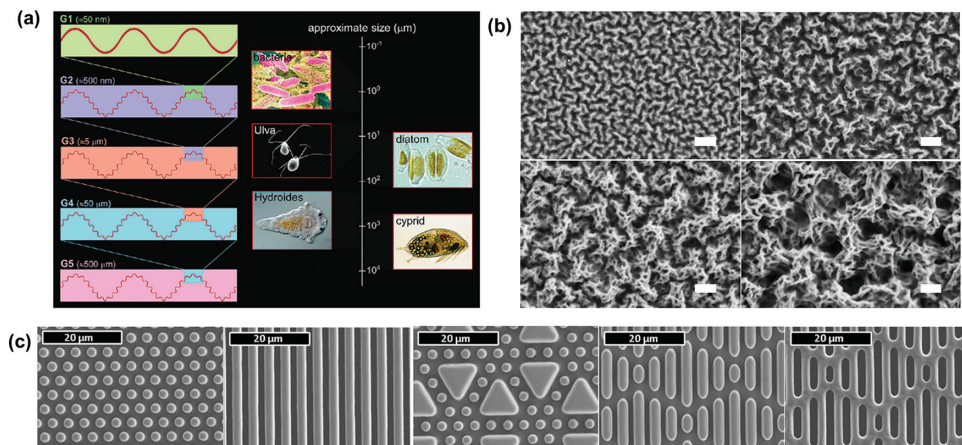


**Figure 6.** Representative surfaces inspired by marine creatures. (a) Schematic illustration of hierarchically wrinkled coatings with nested topography scaled from tens of nanometers to several hundred micrometers. Textures with feature size in certain scale show resistance to the fouling organisms with size in the corresponding scale. Reproduced with permission.<sup>[102]</sup> Copyright 2009, American Chemical Society. (b) SEM images of PAA/PEI multilayer films mimicking the pilot whale (*Globicephalamelas*) skins.<sup>[105]</sup> The feature size can be modulated by changing pH of the solutions. Scale bars: 1 μm. (c) SEM images of surfaces with engineered micro-topographies on PDMS elastomers (from left to right: pillars, ridges, triangle/pillars, Sharklet AF, recessed Sharklet AF). Reproduced with permission.<sup>[106]</sup> Copyright 2010, Springer.

Inspired by mussel adhesive, 3,4-dihydroxyphenyl-L-alanine (DOPA) has made it excellent candidate for plenty of applications.<sup>[112]</sup> DOPA can serve as adhesive to promote adhesion of functionalized polymer to the substrates<sup>[113]</sup> or facilitating anchoring AF molecules onto matrix polymers.<sup>[114,115]</sup> Still, other studies showed that DOPA could act as an alternative of PEG, with both excellent protein resistance<sup>[116,117]</sup> and a capability of almost substrate-independent modification.<sup>[118]</sup>

### 3.3.3. Chemical Defenses

Earlier than the investigation of physical properties of AF models was the exploration of natural antifoulants, mainly including secondary metabolites and enzymes. Nearly 20,000 natural antifoulants have been isolated from marine creatures,<sup>[119]</sup> most of which are proved to be antibacterial, anti-algal, anti-macrofouling or antifungal.

Sponges, soft corals, limpets and algae have been studied as models of chemical strategies against fouling. Müller et al.<sup>[120]</sup> recently reviewed the AF performances of marine sponges. Except that the specular palisade and bio-silica on the surface functionalized in a physical way, biofouling might be prevented through direct killing or indirect inhibition of “quorum sensing” among bacteria during the formation of biofilm by secreting bio-active metabolites. The ASABF-type peptide has been defined as an effective AF compound. Enzyme is another type of biomimetic chemical, which will work by means of degrading the fouling organisms and bioadhesives or generating other biocides. Given that most fouling processes involve the absorption of proteins on the surfaces at first, proteases might be an ideal natural antifoulant. Aldred et al.<sup>[121]</sup> assessed the potential of Alcalase (R) as antifoulant to barnacle cypris larvae. In comparison with other enzymes, proteases also revealed higher effectiveness in inhibition of macrofoulers.<sup>[122]</sup> Through an indirect strategy, another enzymatic

marine coating was fabricated.<sup>[123]</sup> By exposing the coating to seawater, hydrogen peroxide (H<sub>2</sub>O<sub>2</sub>) could be released from the coating and then acted as an environmentally benign antifoulant.

Although natural antifoulants are effective and environmental friendly, the practical application is in a dilemma with questions of the cost, durability, reparability and coating smoothness.

### 3.3.4. Other Strategies

In nature, a great many of self-cleaning processes are carried out in a more active way like dynamic deformation or motion. For example, Shivapooja et al.<sup>[124]</sup> reported an AF approach based on the dynamic changes of surface area and topology of elastomers in response to electromechanical, mechanical and pneumatic stimuli, respectively. This work may enlighten the design of AF coatings in a broader horizon although assistance of other technology is still required for practical applications. Another strategy evolved from biologically behavioral effects, can be described as dynamic eliminating foulers through burying, hiding or crypsis change in salinity and emersion into air.<sup>[120]</sup> In a way, since the active and intelligent mechanisms might be too tough to be realized in the abiotic coating systems, it should be achieved by mechanical cleaning of human beings with subjective initiative.

Marine antifouling is very intricate, facing with complicated fouling species and marine environment. Although potential mechanisms of AF performance in biology systems have been investigated, there is still a long way to go to utilize these bio-inspirations in practical products. Moreover, scientists have become aware of that long-term protection from marine bio-fouling cannot be achieved by only one single strategy. Instead, a combination of several AF methods should be integrated in the final AF systems.

### 3.4. Bio-inspired Anti-reflective Surfaces

In nature, abundant optical phenomena, including broad-angle structural color, antireflection, iridescence, ultra-blackness and -whiteness and light focusing, have attract great research interests.<sup>[125,126]</sup> Endeavors to uncover the relationship between the surface structure and the natural optical phenomena have led to fruitful results based on the development of different microscopy technologies. Diverse 2D architectures have been presented and guided a path of mimicking these evolutionary and sophisticated structures.<sup>[127–132]</sup> Many of them have been realized in manmade surfaces with nanofabrication technology.<sup>[133]</sup> In this section, we focused on antireflective surfaces inspired from natural models.

Along with the flourishing development of electronics, optical devices with antireflective properties are in high demand. In the application of flat panel display or detector, antireflective surfaces can be a solution to decrease reflection and eliminate ghost images or veil glare.<sup>[134]</sup> Besides, the efficiency can be promoted by applying antireflective coating on the surface of solar cell.<sup>[135]</sup> To reach an ideal antireflective

property, several principles should be followed<sup>[136]</sup>: the refractive index of the coating  $n_c = (n_a \times n_s)^{1/2}$ , where  $n_a$  and  $n_s$  are the refractive indices of the air and substrate, respectively; the thickness of the coating should be  $\lambda/4n_c$ , where  $\lambda$  is the wavelength of the incident light. Usually, manmade antireflective surfaces are multilayered films with different reflective indexes, which require a high consumption of raw materials and complicated production processes. While in nature, almost perfect antireflective property can be obtained through just one single layer of nanostructure. It has been confirmed some moths and butterflies utilize periodic nanostructure to achieve antireflection. Taking the corneal of the *polygonia c-aureum* and *lycanidpseudozeeriamaha* for instance (Figure 7), the sub-300-nm nipple arrays on the corneal surface can provide a transition with gradual change of refractive index between the air and the bulk eye, thus reducing the reflectance of incidence light. In this case, the resultant reflection can be divided into infinite series of reflection,<sup>[137]</sup> each with a different phase, at each incremental change in index. Once the transition takes place at an optical distance exceeding  $\lambda/2$ , the reflectance would reduce and even fall to zero.<sup>[133]</sup>

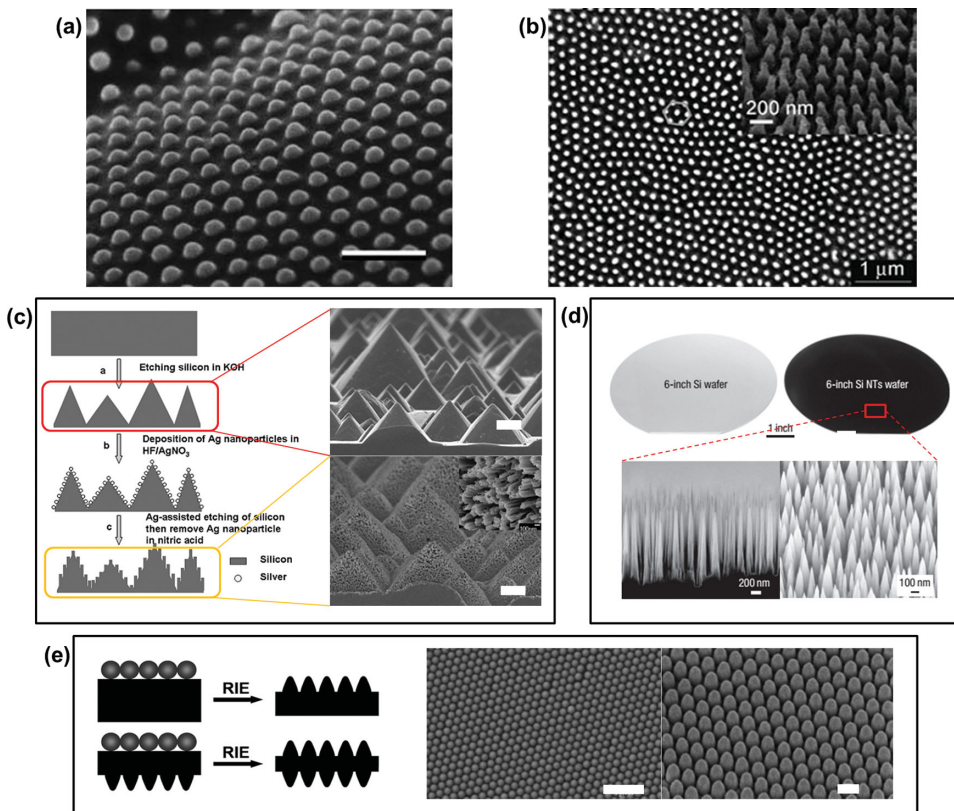


**Figure 7.** Nipped arrays of biological systems and biomimetic antireflective surfaces fabricated by top-down techniques. SEM images of (a) corneal of *lycanidpseudozeeriamaha*,<sup>[138]</sup> and (b) cicada wing.<sup>[129]</sup> Reproduced with permission.<sup>[138]</sup> Copyright 2006, Royal Society of Chemistry. (c) Hierarchical, pyramid-like nanostructure prepared by KOH and Ag-assisted etching of silicon: left shows fabrication process; right shows the corresponding morphology of the surface (scale bars in the SEM images are 2 μm).<sup>[139]</sup> (d) Photographs (top) and SEM images (bottom) of antireflective Si wafer by a high-density electron cyclotron resonance (ECR) plasma etching. Reproduced with permission.<sup>[140]</sup> Copyright 2007, Nature Publishing Group. The photo top exhibits the comparison of bare Si wafer with Si NTs (nanotips) wafer. (e) Fabrication of antireflective surface with uniform nipples by colloidal lithography. The left schematic diagram shows the preparing process. The right two figures show the morphology before and after etching.<sup>[141]</sup> Based on this structural feature and mechanism, both top-down etching and bottom-up assembly were developed to fabricate bio-inspired antireflective surfaces.

### 3.4.1. Top-Down Methods

Lithography<sup>[142–145]</sup> is one of the most often used top-down methods, through which various high-performance, nanostructured AR surfaces have been fabricated. The most attractive advantage of top-down technique is its capability of forming randomly ordered shapes of nanostructure. To improve the antireflective properties of nanostructured surfaces, high aspect ratio was believed to be crucial.<sup>[146]</sup> Huang et al.<sup>[140]</sup> reported aperiodic silicon nanotips array of on a sub-wavelength structured wafer that can suppress the light reflection from the ultraviolet to the terahertz region. By high-density electron cyclotron resonance plasma etching, silicon nanotip arrays formed on the surface of wafer, with a base diameter of 200 nm and adjustable lengths from 1 to 16 μm (Figure 7d). A similar silicon hollow-tip arrays with high aspect ratio was fabricated by Li et al.<sup>[147]</sup> Except for the excellent AR property with a specular reflectance lower than 1% in the 250–1600 nm range, the arrays also exhibited a good repellence to water droplet. A room temperature nanoimprint lithography method was developed to fabricate ordered arrays of sub-wavelength hydrogen silsesquioxane nanorods.<sup>[148]</sup> The as-prepared moth-eye type nanorod arrays exhibited superior omnidirectional antireflection characteristics in visible wavelengths. Colloidal lithography has also been emphasized due to the time-effective and reproductive merits.<sup>[141,151]</sup> In this process (as illustrated in Figure 7e), colloidal particles are first arranged on the surface to form a uniform 2D coating, and then nipples came into being after etching. Cone-like structure may be obtained after further etching.

Another effective route is replica moulding of the surface of original model. The advantages compared with lithography method are cost effective and relatively easy to implement. A direct replication route was used to prepare compound-eye-like antireflective coatings, which was reproducible and promising in large-area substrate application.<sup>[149]</sup> Template-mediated UV replica molding was utilized to fabricate robust and non-fouling antireflective coatings on large-scale solar cells.<sup>[150]</sup> In addition, chemical etching was a promising technique as well for large-scale production of antireflective surfaces. KOH was usually used as etchant for silicone substrates and pyramids-like<sup>[139]</sup> (Figure 7c) and nano-wires<sup>[140]</sup> morphologies could be created. This electroless etching was simple and cost-effective.

### 3.4.2. Bottom-Up Methods

Bottom-up routes for fabricating antireflective coatings have also been intensively studied because of their facility and great potential in large-scale applications. Nanoporous materials are the most popular candidates. SiO<sub>2</sub> nanoparticles and sol are usually used as precursors for antireflective coatings because of their adjustable refractive index, good durability and environmental resistance.<sup>[152]</sup> By means of modulating the parameters of nanoparticle or sol, excellent antireflective properties can be obtained. Among various silica nanoparticles, mesoporous silica nanoparticles are the most popular options because of their hierarchical structure (Figure 8a).<sup>[153–156]</sup>

Sol-gel<sup>[157,158]</sup> and layer-by-layer<sup>[159]</sup> processes are always involved in the formation of antireflective films constructed by silica nanoparticles. There are some other efforts devoted to exploring facile and feasible methods to improve the mechanical properties of nanoparticles-formed films.<sup>[158,160,161]</sup> In a recent study, plasma-enhanced chemical vapor deposition (PECVD) was utilized to prepare antireflective coating in one step and the antireflective coating obtained exhibited good durability to high level strains (Figure 8b).<sup>[162]</sup>

Preparation of AR coating by a facile method in large scale is a key issue for the practical application. Xu et al. developed a roller coating technique to prepare silica nanoparticles formed antireflective coatings on patterned glass and then applied the AR glass on photovoltaic modules (1580 × 808 × 35 mm) (Figure 8c).<sup>[136]</sup> Nowadays most of the AR glass for solar cells have been mass produced by roller coating.

Bio-inspired antireflective surfaces have been developed in both top-down and bottom-up solutions in recent years. Given different application backgrounds, other aspects including mechanical property, wettability, cost and feasibility of the technique involved should be considered. As novel techniques keep emerging, more ideal biomimetic antireflective surfaces could be expected in the near future.

## 4. Bio-inspired Three Dimensional Materials

### 4.1. Damping Materials with Bio-inspired Structures

For damping materials, the energy absorption capacity is often expressed by loss tangent ( $\tan \delta$ ), which is defined by the ratio of the storage moduli ( $E'$ ) to the loss moduli ( $E''$ ).<sup>[163]</sup> For practical applications, the damping materials are required to possess both a high damping peak value and broad effective damping temperature and frequency range. In general, a good damping material should show a  $\tan \delta$  value higher than 0.3 in a temperature range over 60 °C. Although a lot of efforts have been made to improve the damping capabilities of manmade materials, it is still difficult to meet the practical demands, especially in some particular fields, such as aerospace and electronics.<sup>[164,165]</sup> Therefore, many researchers begin to mimic the principal of the structure design in biological composites to obtain the desired high damping materials.

The spatial gradients in composition and/or structure are of considerable interest in the design for damping materials, because the continuously changing composition or microstructure can minimize interfacial stresses and reduce stress concentration at any point, thus increasing mechanical toughness and enhancing energy dissipation for vibration control and impact resistance.<sup>[166]</sup>

Gradations in microstructure and/or porosity are commonly observed in biological structures like plant stems and bones.<sup>[167]</sup> A typical example is the pummelo fruit (*Citrus maxima*) which drops from heights of 10 m or more without being destroyed.<sup>[168]</sup> The foam-like peel with 2 to 3 cm in thickness has been proved to play an important role in the impact resistance. The peel is capable of dissipating considerable amounts of kinetic energy due to its gradient porous hierarchical structure (Figure 9a–c). The energy absorption performance of pummelo peel has been

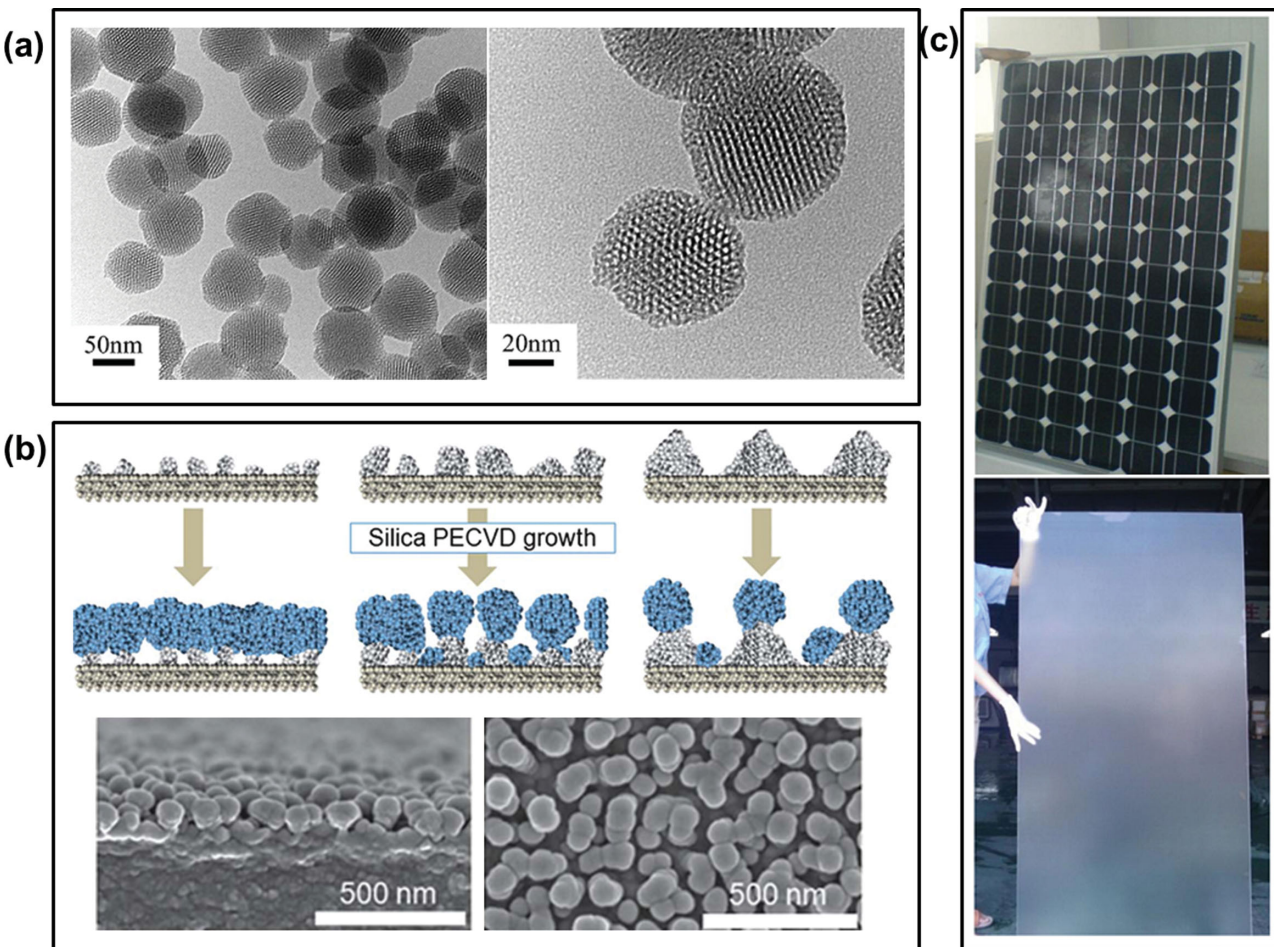


**Figure 8.** Several representative studies of antireflective surfaces based on bottom-up technique. (a) TEM images of spherical mesoporous silica nanoparticles that used to form antireflective coatings. Reproduced with permission.<sup>[155]</sup> Copyright 2010, American Chemical Society. (b) Preparation of antireflective film by single-step plasma-enhanced chemical vapor deposition (PECVD): top shows schematic diagram of silica PECVD growth process; the bottom ones show cross-sectional (left) and plane (right) SEM images of as-prepared antireflective coating after 3-minute pretreatment by plasma. Reproduced with permission.<sup>[162]</sup> Copyright 2012, Royal Society of Chemistry. (c) The manufactured silicon solar modules (top, size: 1580 × 808 × 35 mm) and photos of the cover glass with the silica coating (bottom). Reproduced with permission.<sup>[136]</sup> Copyright 2011, Elsevier.

widely studied by many researchers.<sup>[18,168]</sup> However, preparation of pummelo peel inspired damping materials is rarely reported. Fischer et al.<sup>[18]</sup> successfully transferred the pummelo peal like hierarchical structure to 3D engineering metal foam structures by a modified investment casting process (Figure 9d). The developed alloy Bi57Sn43 showed enhanced damping and impact resistance properties.

Mussel byssus<sup>[169–171]</sup> and tendon,<sup>[172]</sup> having typical gradually changing composition, also provide us inspirations. These stiff-soft gradient biological structures adjoin soft and stiff constituents, transfer loads and avoid stress concentration. Mussel byssus is used to attach mussel to rocks (Figure 9e). The byssus shows a gradually changing elastic modulus from the proximal part (50 MPa), which connects to the soft mussel tissue, to the distal part (500 MPa) connected to stiff stone surface (Figure 9f). It is the mechanical gradation that enables the mussel byssus act as an effective shock-damper against the impact force. Tendon is also a prominent stiff-soft gradient tissue to link soft muscle tissue with stiff bone. The gradients can help tendon more effectively damp damaging vibrations generated in the

leg as the animals run. Following the structure design rules, a gradient 3D elastomer network of styrene/butadiene rubber was prepared by the sulfur diffusion and then vulcanization.<sup>[173]</sup> The obtained polymer with a gradient from rubbery to glassy phase exhibited a wide transition range spanning over 100 °C (Figure 9g).

Furthermore, gradient interpenetrating polymer networks (g-IPNs) with a continuously changing composition are excellent candidates as damping materials. It was demonstrated that g-IPNs could remarkably broaden the effective damping temperature range compared to traditional IPN. For example, polyurethane/vinyl ester resin g-IPNs were synthesized by sequential curing and a broader effective damping temperature ranging from -57 to 90 °C ( $\tan\delta > 0.3$ ) was observed.<sup>[174]</sup> The gradient semi-IPNs based on polyurethane and PVP showed broader glass transitions and enhanced moduli compared with traditional semi-IPNs.<sup>[175]</sup>

Novel lightweight microframe structural materials are attractive candidates for mechanical applications for providing high stiffness, strength and energy absorbing capabilities due to the

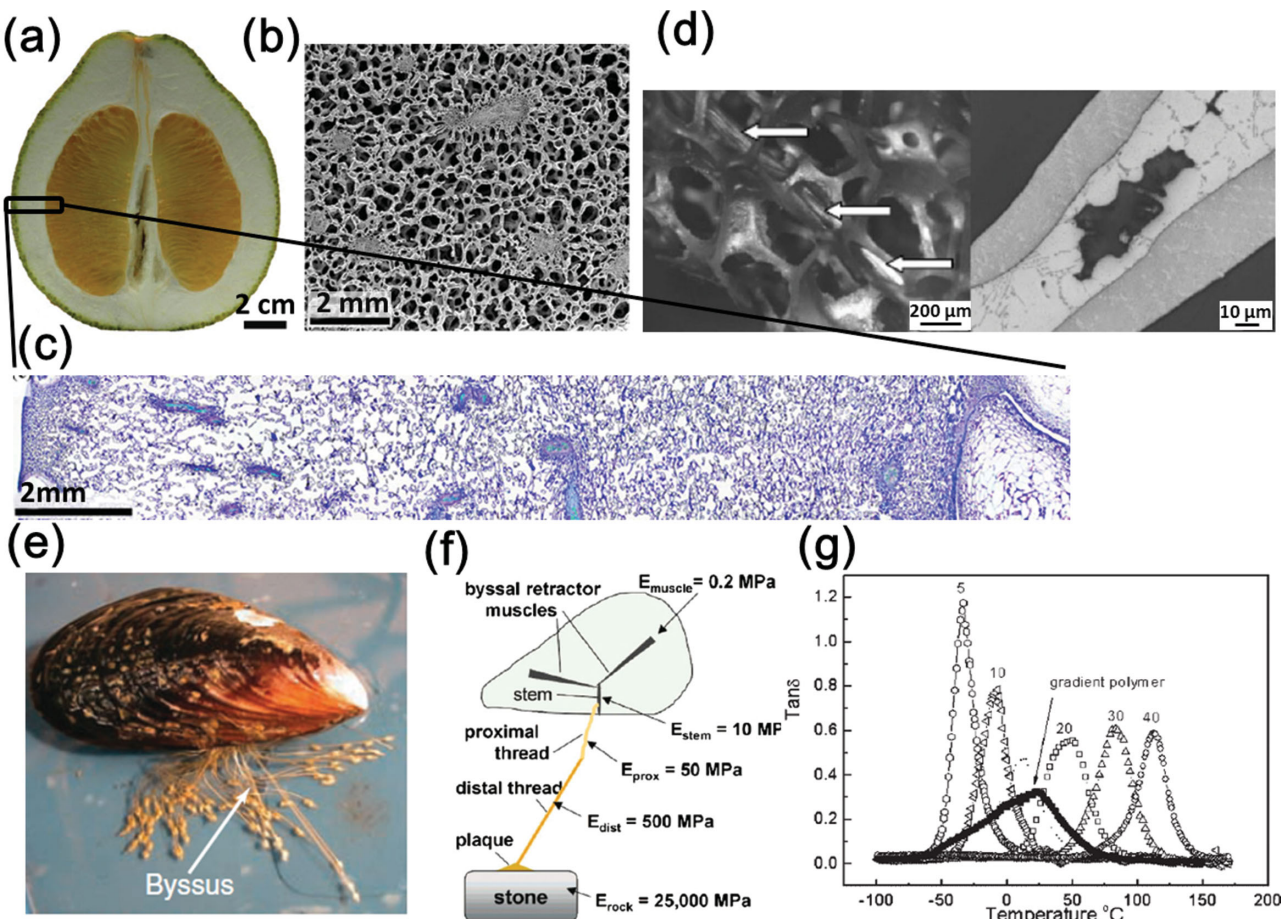


**Figure 9.** (a) Photograph of the longitudinal section through a pummelo fruit (*C. maxima*), revealing the extraordinary thick peel. (b) SEM image of the albedo tissue showing the foam-like structure. (c) Thin-section (8  $\mu\text{m}$ ) of a pummelo peel sample, stained with toluidine blue. The peel is permeated by vascular bundles and its density gradually changes from the epidermis (left) towards the fruit pulp (right). Reproduced with permission.<sup>[168]</sup> Copyright 2013, Springer. (d) The hierarchical structures of pummelo peel inspired metal foams: long fiber reinforced open pore metallic foam (left, white arrows: fiber bundle), and sponge strut with secondary porosity and two different materials (right,  $\text{Bi}_{57}\text{Sn}_{43}$  outer and  $\text{AlSi}_7\text{Mg}$  inner material).<sup>[168]</sup> (e) Photograph of mussel byssus composed of numerous extensible, shock absorbing byssus threads. Reproduced with permission.<sup>[170]</sup> Copyright 2010, AAAS. (f) Schematic mussel byssus attached to a stone, showing a gradient changing elastic modulus from the proximal part (50 MPa) to the distal part (500 MPa). Reproduced with permission.<sup>[169]</sup> Copyright 2004, American Chemical Society. (g)  $\tan \delta$  vs. temperature for a gradient polymer and for SBR with different sulfur contents. The gradient polymer shows a broader transition range compared with conventional SBR vulcanizates.<sup>[173]</sup>

size scale dependent mechanical properties.<sup>[176]</sup> Microframe structures appear widely in nature, such as *Euplectella* sp. skeleton<sup>[177]</sup> and sea urchin exoskeleton,<sup>[178]</sup> which endow them superior mechanical properties. The skeleton of *Euplectella* sp. shows macroscopic cylindrical square-lattice cage-like structure formed by hierarchical assembly of the constituents from nanometer to macroscopic scale (Figure 10a,b). The unique biological structures are believed to contribute to the outstanding mechanical rigidity and stability of the sponge skeleton, which inspires material scientists to mimic the structures to create novel lightweight energy absorption materials.

Recently, 3D periodic sub-micrometer frame architectures have been made and widely studied as potential damping materials due to the enhanced energy absorption per unit of mass, or specific energy absorption (SEA). Thomas' group has done beautiful work for the development of microframe structures.<sup>[179–185]</sup> Jang et al. created 3D epoxy (SU-8) micro-frames by using laser interference lithography.<sup>[179]</sup> These periodic

porous polymer/air structures exhibited unusually large plastic deformations with local failure strains reaching ca. 300% due to their length-scale-dependent mechanical behavior, which make them become underlying new structures for energy absorption. The plastic dissipation and mechanical response of SU-8 microframe using micromechanical modeling were further quantitatively investigated.<sup>[181]</sup> It works out how to optimize the material structure for maximum energy absorption. Subsequently Lee et al.<sup>[182]</sup> experimentally studied the plastic deformation mode and energy absorption as a function of relative density. The results showed that the epoxy nanoframe can absorb more energy per unit volume when the relative density is low. What is worth mentioning, Wang et al.<sup>[183]</sup> used the polymer micro-frames as matrix to develop layered structure composites consisting of staggered mineral platelets embedded in polymer micro-frames, inspired by the three dimensional brick-and-mortar structures in nacre. The hierarchical structures showed a significant enhancement in volume energy dissipation, due

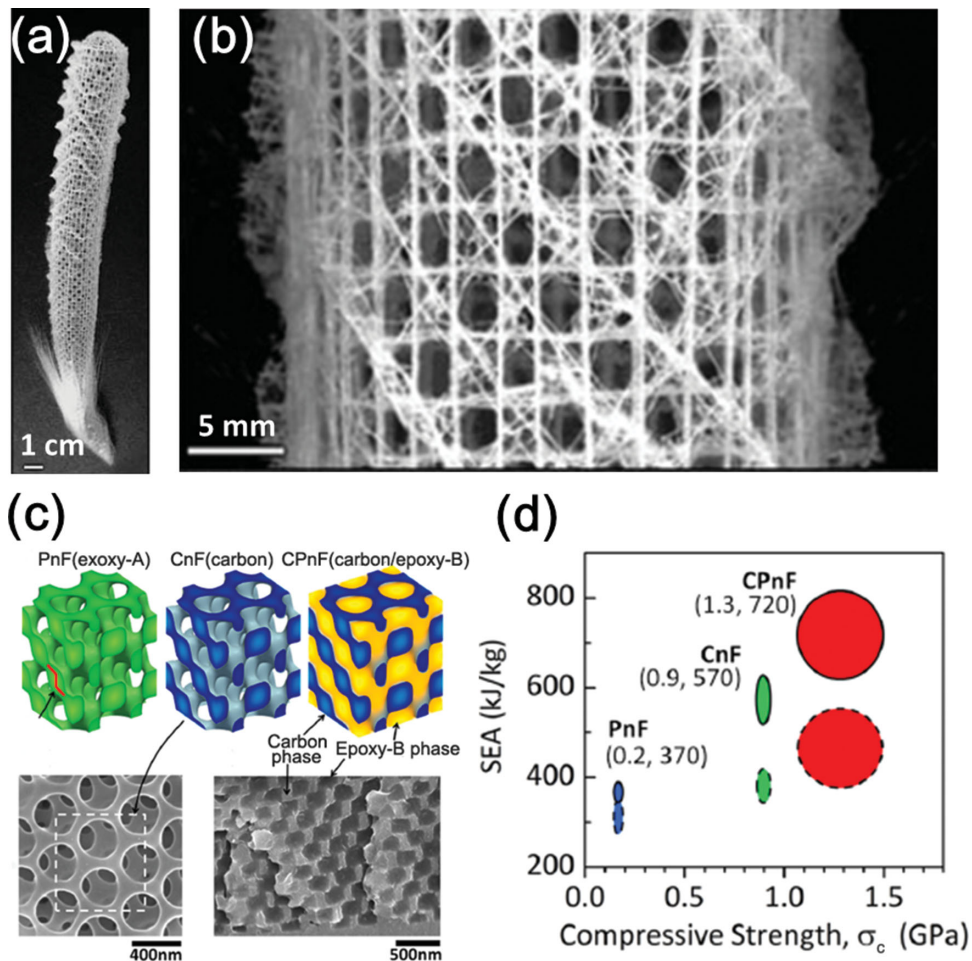


**Figure 10.** (a) Photograph of the entire *Euplectella* sp. skeleton, showing cylindrical glass cage. (b) Fragment of the cage structure showing the square-grid lattice of vertical and horizontal struts with diagonal elements arranged in a chessboard manner. Reproduced with permission.<sup>[177]</sup> Copyright 2005, AAAS. (c) Top shows perspective illustration of  $1 \times 2$  cells for three types of nanoframes: PnF, CnF and CPnF. Bottom left shows a top view SEM image of a CnF; periodic interpenetrating carbon and epoxy-B phases are shown in a SEM image of a tensile fractured surface of a CPnF (bottom right). Note the excellent filling by the epoxy-B and the absence of voids. (d) Ranges of the upper limit (solid line) and lower limit (dashed line) of SEA of the three materials versus compressive strength. Reproduced with permission.<sup>[185]</sup> Copyright 2012, American Chemical Society.

to the lateral expansion of microframe polymer mortar and the load transfer to mineral bricks during plastic deformation.

The combination of hard and soft materials has usually been used to enhance energy dissipation in natural structures. Inspired by this design principals, two or more phases can be combined to create periodic bi- or multi-composites, despite the initial periodic porous structure with a single solid phase. For example, 3D periodic glassy polymer/rubbery polymer co-continuous composites with different geometric arrangements were fabricated using a 3D printer, which showed high specific energy absorption in all directions.<sup>[184]</sup> Recently, carbon/epoxy periodic bicontinuous nanoframes, composed of interlocked hard (carbon) and soft (epoxy) phases, were prepared by infiltration of CnF with epoxy-B monomer (Figure 10c).<sup>[185]</sup> It has been shown that this bicontinuous composite has significantly improved energy absorption with an extremely high specific energy absorption (SEA) up to 720 kJ/kg (Figure 10d).

In periodic bi-continuous composites, 3D interlocked phase interactions, such as stress transfer and strain sharing, are

responsible for the increase in failure strain and energy absorption. In addition, the mechanical behavior and energy absorption of the co-continuous composites can be tailored by controlling volume fraction, changing the constituents and geometric arrangements for a wide range of applications.

The sophisticated 3D hierarchical structures endow the biological materials outstanding damping properties by unique mechanical deformation mechanism. Although the gradient and micro-frame architectures have been studied and mimicked to create novel high energy absorption materials, the relevant research is still in the premature stage. Other strategies in the function of biological damping structures, such as the sole of polar bears, the paw of puma, need to be uncovered through detailed structural composition and mechanical characterization. As limited by the current technology, the manmade structures are quite simplistic compared with the sophisticated structures in natural prototypes. Otherwise, theoretical modeling should be established to predict the energy absorption capability, which can help to

better understand the relationship between the structures and damping properties.

#### 4.2. Aerogels: Amazing 3D Structured Ultralight Porous Materials

Aerogels are a family of 3D structured porous materials, which are generally dried from gels using specific technique. Featured by low density, large porosity, high specific surface area and low thermal conductivity, aerogels have drawn great interests in a wide range of applications.<sup>[186]</sup> The first prepared and also the most classic aerogels are supercritical-dried silica aerogels.<sup>[187]</sup> However, the fragility of the aerogels stemming from the porous skeleton and the laborious supercritical CO<sub>2</sub> drying technique restricts the practical application of aerogels in many fields.<sup>[188]</sup> Up to date, new precursors to build the wet gels, facile drying methods to replace the liquid in the wet gels by air, and enhanced durability of the resultant aerogels for practical application are the main topics for aerogel research.<sup>[189–194]</sup>

Recently, by virtue of the intensive exploration of graphene and carbon nanotube and the inspiration from biomaterials, carbon aerogels have drawn great research interests.<sup>[195]</sup> Having retrieved the record of the lowest density solid material<sup>[196]</sup> (**Figure 11a**) from the ultralight metallic microlattices,<sup>[197]</sup> carbon aerogels show several unique performances because of their high electrical conductivities and superior mechanical properties.<sup>[198]</sup> Generally, there are two strategies to prepare

carbon aerogels: one is to carbonize the cross-linked wet gels to carbonaceous gels and then freeze-dried to aerogels, and the other is to assemble carbon materials into gels first and then dried to carbon aerogels.<sup>[199]</sup>

The recent progresses in the fabrication and application of aerogels have been summarized by Du and Dorcheh in their review articles.<sup>[200,201]</sup> Herein, we focus on the development of preparation of aerogels from biomaterials.

As being easy to get, renewable, low cost and nontoxic to humans, biomaterials have been considered increasingly as precursors for the preparation of aerogels. Besides, biomaterials are inherently beneficial since they are generally in gel state. The traditional sol-gel transition is not involved in the fabrication of aerogels using biomaterials as the raw materials, largely simplifying the preparation procedure. Therefore, carbon-rich biomaterials are ideal candidates as the precursors for carbon aerogels. For example, bacterial cellulose, watermelon, raw cotton, chitin and chitosan have been successfully used to prepare aerogels.<sup>[202,203]</sup>

Watermelon is a new carbon source to produce aerogels (**Figure 11b**).<sup>[204]</sup> After a simple one-pot hydrothermal reaction carried out at 180 °C for 12 h, flexible and chemically active gels are obtained. The carbonaceous gels are good scaffolds to synthesize 3D composite materials and are feasible to be freeze-dried directly to carbon aerogels. Wu et al. also reported a facile method to fabricate fire-resistant carbon aerogels from bacterial cellulose (**Figure 11c, d**).<sup>[205]</sup> The bacterial cellulose was firstly freeze-dried and then sintered at 700–1300 °C under argon

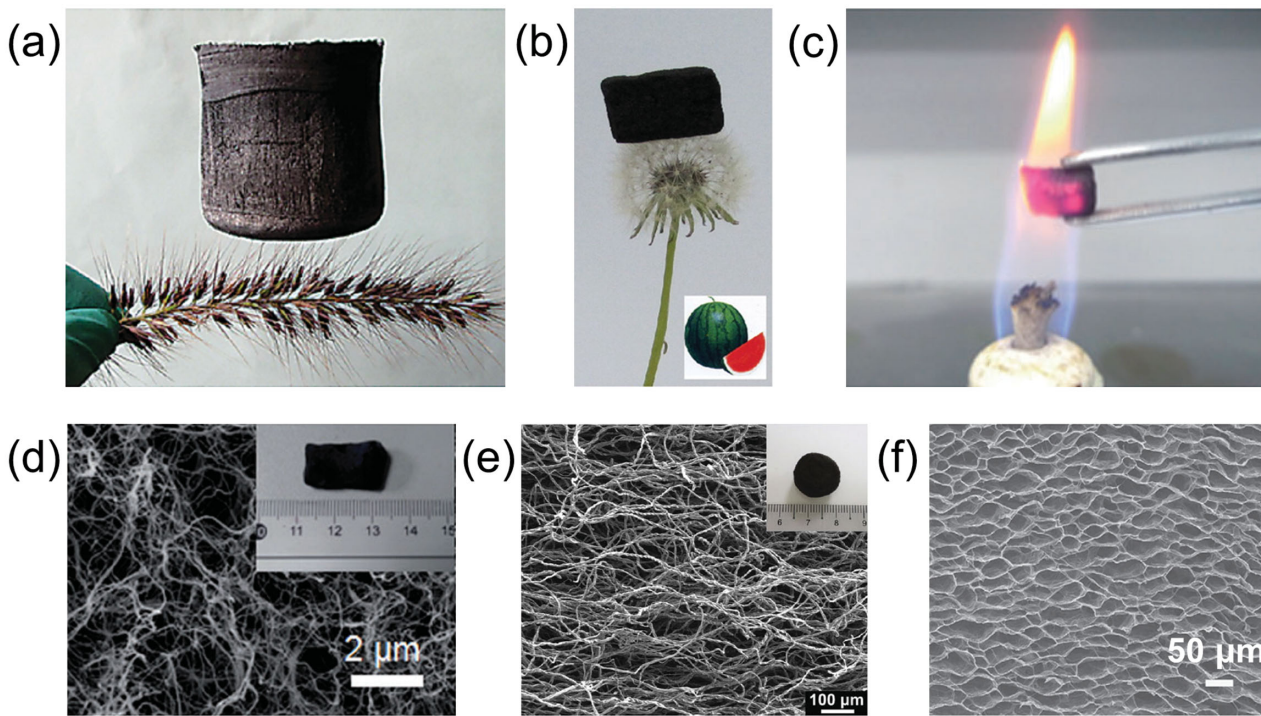


**Figure 11.** (a) Photograph of an ultra-flyweight aerogel standing on a setairaviridis.<sup>[196]</sup> (b) Image of a carbon aerogel derived from watermelon held by a dandelion. Reproduced with permission.<sup>[204]</sup> Copyright 2013, American Chemical Society. (c) Picture of a carbon aerogel from bacterial cellulose demonstrating its fire-resistance.<sup>[205]</sup> SEM images of the carbon aerogels derived from (d) bacterial cellulose,<sup>[205]</sup> (e) raw cotton.<sup>[206]</sup> Insets are digital images of the corresponding aerogels. (f) SEM image of the top view of the honeycomb-like graphene aerogels mimicking the structure of natural cork. Reproduced with permission.<sup>[207]</sup> Copyright 2012, Nature Publishing Group.

atmosphere, and ultralight carbon nanofiber aerogels with densities of 4–6 mg cm<sup>-3</sup> were obtained at a large scale.

Raw cotton, a native porous 3D network already filled by air, is a promising raw material for synthesizing carbon aerogels because it does not need a drying process. Bi et al. reported that twisted carbon fibers (TCF) aerogels could be simply obtained by pyrolyzing raw cotton at 800 °C under low pressure argon atmosphere (Figure 11e).<sup>[206]</sup> Although serious shrinkage occurs during the pyrolysis process, the resulting aerogels still have a low density of about 12 mg cm<sup>-3</sup>. The good mechanical property and hydrophobicity of the TCF aerogels are advantageous for practical applications.

Biomaterials also provide inspirations for the fabrication of aerogels with special architectures. Inspired by natural cork, Qiu and coworkers prepared super-elastic graphene-based aerogels with a honeycomb-like hierarchical structure (Figure 11f).<sup>[207]</sup> The aqueous dispersion of partially reduced graphene oxide (pr-GO) was freeze cast, and the pr-GO sheets stacked at the ice crystal boundary and then aligned along the growth direction of ice, leading to the formation of a continuous honeycomb-like skeleton. The hexagonal structure has been proven to benefit maximizing bulk-specific elastic modulus.<sup>[208]</sup> Thus the resulting monoliths exhibit superelasticity with an extremely high recovery rate and can bear a load more than 50 000 times of their own weight. Xu et al. also acquired porous graphene aerogels with a similar aligned structure by spinning liquid crystalline graphene oxide into liquid nitrogen. The as formed aerogels had excellent specific mechanical strength as well.<sup>[209]</sup>

Traditionally, supercritical drying has been recognized as the most effective method for drying gels to form aerogels, because this technique has no liquid/gas interfaces and prevents the pore structure from collapsing during the drying process.<sup>[210]</sup> In contrast, freeze-drying is a much more convenient method which also avoids the liquid/gas phase boundaries.<sup>[211]</sup> But freeze-drying has rarely been used for the preparation of classic aerogels because the solvent crystallization in the pores would destroy the gel network into powders.<sup>[186]</sup> However, for drying carbonaceous gels, freeze-drying revitalizes and shows its versatility, not only as a low cost technique, but also as an ordered structure producer. The difference in the networks between conventional and carbonaceous gels determines the validity of freeze-drying. The architectures of aerogels derived from graphene, CNT and other carbon sources are continuous in extended 1D or 2D scale. The networks of common silica aerogels, for example, are constructed by nanoparticles stacked point to point. Additionally, carbon materials, especially graphene and CNT, have superior mechanical properties with the elastic modulus on the order of 1TPa. The continuous and robust network is much more tolerant than the particle stacked network when being squeezed by the growth of solvent crystal. Therefore, carbon aerogels can be conveniently prepared using freeze-drying.

With abundant source of precursors from nature and convenient drying method, bio-inspired carbon aerogels are now available to be produced in large scale. Benefited from the inherent unique properties, including excellent mechanical property, electrical conductivity etc., carbon aerogels have demonstrated potential applications in many fields. It has been illustrated that the superelastic graphene-based cellular

aerogels possess high energy absorption capability.<sup>[207]</sup> Thanks to the electrical conductivity and the large specific surface area, carbon aerogels have also been used as pressure sensitive conductors<sup>[257]</sup> (Figure 12a) and supercapacitors.<sup>[204]</sup> In addition, Bi,<sup>[206]</sup> Wu<sup>[205]</sup> and their colleagues have demonstrated the application of carbon aerogels as efficient and recyclable collectors for oils and organic solvents (Figure 12b,c).

The facile freeze-drying method and the excellent mechanical performances promise carbon aerogels a broad range of fascinating applications. However, there is still a long way to go for aerogels to be widely applied in our daily life. The lightweight porous materials are not robust enough to bear an impact even though they have shown improved performances under quasi-static compressions. In future, to seek convenient drying technique and to build tough enough structures remains challenging. Very recently, Xu et al.<sup>[212]</sup> reported the preparation of robust aerogels derived from a thioether bridged silsesquioxane by a straightforward Vacuum-Drying method. The drying method is much more convenient than the conventional supercritical drying, ambient pressure drying and even the freeze-drying, though the availability of the method for other precursors still needs to be investigated. The excellent robustness and facile preparation procedure of the aerogels promise wide practical applications. Finally, there are still plenty of opportunities to explore many other natural materials as the precursors for the fabrication of silica aerogels, carbon aerogels or aerogels with other compositions.

#### 4.3. Stimuli-Responsive Actuators Based on Hydrogels

Living organisms in nature, from bacteria to humans, are moving all the time. Movements or deformations along with time, usually as responses to environmental stimuli, are intrinsic properties of organisms and also attractive inspirations for manmade actuators. The manmade muscle-like actuators based on hydrogels with stimuli responsive functions will be mentioned in this section.

Hydrogels, which are 3D polymer networks filled with water, can reversibly swell and shrink in response to external stimuli such as temperature, pH value, electric field and light.<sup>[213–215]</sup> When environmental conditions altered, hydrogels are capable of undergoing large deformations accompanied with the change of water content. Thus hydrogels have aroused increasing interests as promising candidates for biomimetic actuators.<sup>[216,217]</sup>

Jiang and colleagues<sup>[218,219]</sup> used stimuli-responsive hydrogels to construct artificial ciliary muscles that can dynamically adjust the focal length of liquid microlenses (Figure 13a). In their work, a micro-channel system was filled with water, above which a layer of oil was placed. A hydrogel ring incorporated within the micro-channels formed an aperture and the water-oil interface resulted in a liquid micro-lens. The top surface of the aperture was hydrophobic, whereas the side wall and bottom face was hydrophilic. The wettability differences allowed the water-oil interface to be pinned along the aperture periphery. When an appropriate environmental stimulus was applied, the hydrogel ring would shrink or expand, followed by the volume change of the enclosed water. The water-oil interface then moved to another position, resulting in the change of

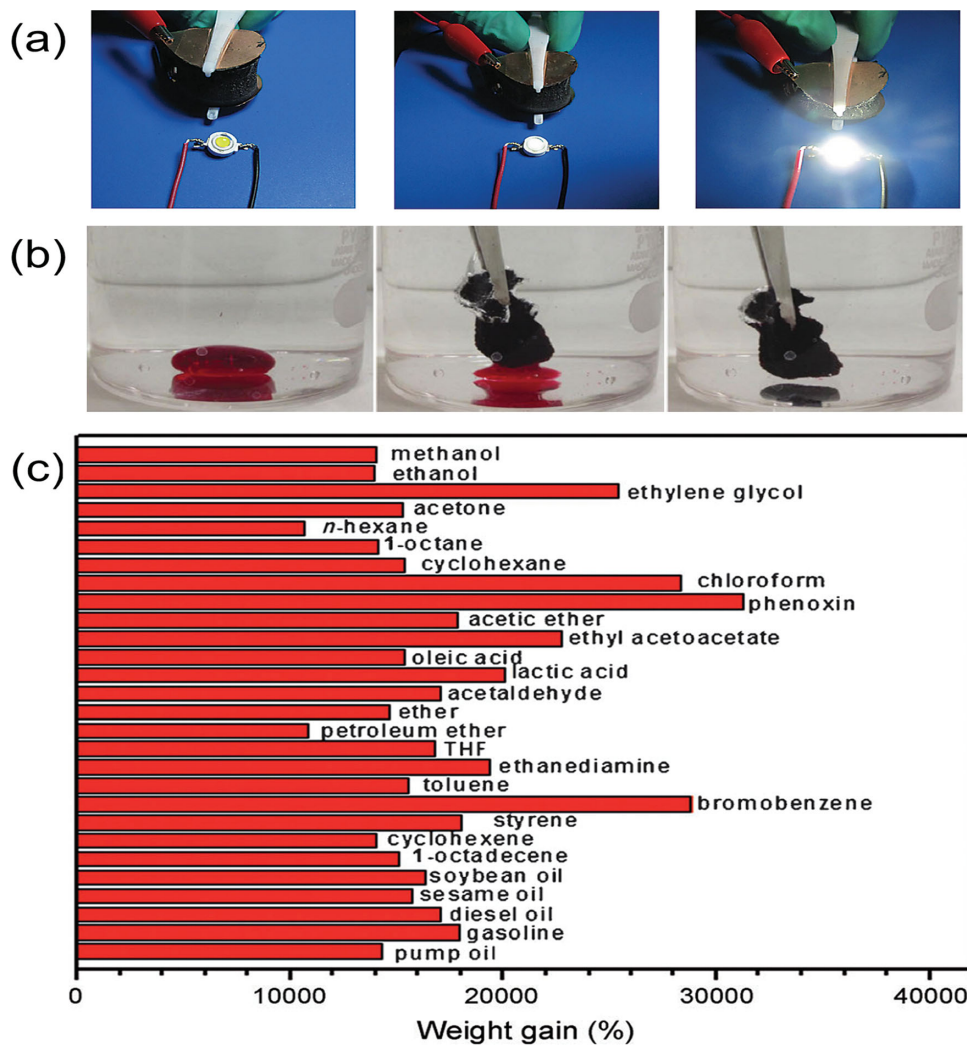


**Figure 12.** (a) Snapshots demonstrating the application of a piece of synergistically assembled carbon aerogel as a press sensitive conductor.<sup>[196]</sup> (b) Snapshots showing collecting dyed organic solvent at the bottom of water by a TCF aerogel derived from raw cotton.<sup>[206]</sup> (c) Absorption efficiency of the carbon aerogels from bacterial cellulose for various organic liquids.<sup>[205]</sup>

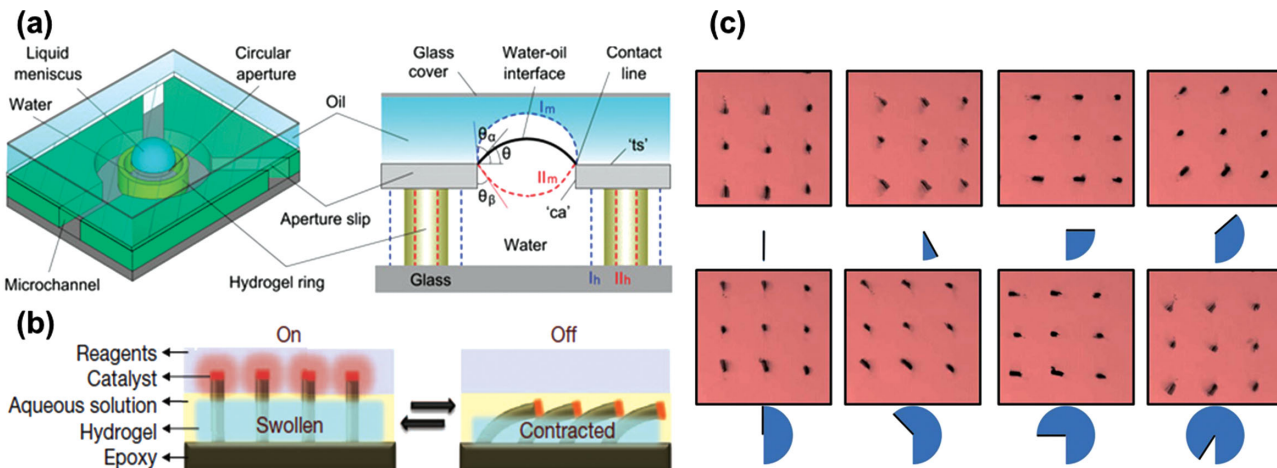


**Figure 13.** (a) Illustration of a hydrogel ring mimicking the ciliary muscles to adjust the focal length of liquid microlens, based on the expansion and contraction of the hydrogel with the local environmental condition change. Reproduced with permission.<sup>[218]</sup> Copyright 2006, Nature Publishing Group. (b) Schematic of the design of self-regulated mechanochemical adaptively reconfigurable tunable system. Reproduced with permission.<sup>[223]</sup> Copyright 2012, Nature Publishing Group. (c) The rotation of artificial hydrogel cilia in response to an external rotating magnetic field.<sup>[224]</sup>

focal length of the micro-lens. In this approach, the role of the hydrogel ring was close to ciliary muscles that help human eyes adjust the focal length by tuning the lens shapes.

Aizenberg et al.<sup>[220–222]</sup> constructed a hybrid actuating system in which hydrogels acted as muscle-like actuators. Silicon or polymer microposts were embedded in a hydrogel layer. The swelling/collapse of the hydrogel in response to humidity change would induce the movements of the microposts. Recently they further developed this system by introducing a catalyst and using thermo-responsive hydrogels (Figure 13b).<sup>[223]</sup> The catalyst was fixed on the top of microposts. When the hydrogels were swollen by water, the microposts kept straight and lift the catalysts to the upper layer where an exothermic reaction was triggered. The temperature of the system increased until the hydrogel microposts bended due to the contraction at high temperature. Then the reaction would be terminated with no catalyst supplied. Consequently the temperature decreased and the hydrogels became swollen again. Through such a continuous feedback loop, the system was able to maintain the temperature in a narrow range. This self-regulated oscillating system has provided an intriguing example mimicking the homeostatic abilities of living organisms.

The actuating systems presented above have employed hydrogels as the “active” components to drive the movements of the “passive” parts of the system. Other than that, a hydrogel actuator itself can be driven to undergo substantial movements. Mendes et al.<sup>[224]</sup> constructed hydrogel arrays with high aspect ratio, namely artificial cilia. The hydrogel cilia were responsive to pH value and electric field. When exposed to an external rotating magnetic field, the cilia filled with magnetic iron particles rotate rapidly (Figure 13c). Xu et al. has recently developed a hydrodynamically driving system in which submerged hydrogels could be passively propelled to move directionally or undergo sophisticated path-finding movements.<sup>[225]</sup>

Inhomogeneous structure is another remarkable feature available for stimuli responsible biomaterials.<sup>[226]</sup> The structural inhomogeneity will lead to different volume or shape change during water absorption/release.<sup>[227,228]</sup> The coupling of the inhomogeneous structure and the stimuli-responsive property of hydrogels will largely enrich the functions and applications of hydrogel actuators. In 1995 Hu et al.<sup>[229]</sup> reported the actuation of a bilayer hydrogel, in which one layer was thermo-responsive and the other layer was not. Thus the hydrogel would bend in response to a temperature change. A variety of hydrogel actuators with multilayer<sup>[230,231]</sup> or gradient structures<sup>[232–234]</sup> have then been developed. Recently Liu and co-workers<sup>[235]</sup> constructed thermo-responsive hydrogels composited with multi-dimensional-gradient magnetic nanoparticles (MNP). The MNP distribution in the hydrogel was set by applying magnetic field before polymerization. As the variations of magnetic field were diverse, the MNP gradients could be designed, resulting in composite hydrogels with “programmable” responsive shaping behavior. Ionov et al.<sup>[236–238]</sup> fabricated stimuli-responsive bilayer hydrogels with carefully designed geometry, which formed various 3D structures by origami-like self-folding.

While hydrogel actuators have exhibited their merits of flexibility and responsiveness, there are some limitations for hydrogels, such as lack of sufficient strength, fast evaporation of water, and relatively slower response due to the diffusion

process.<sup>[216,217]</sup> Elastomers such as silicone rubber and liquid crystals have better performances in these aspects.<sup>[239–243]</sup> Dielectric elastomers, which are electrically responsive materials, have also shown advantages in the artificial muscle applications but huge electric fields are needed.<sup>[244–246]</sup> Recently, deBotton has demonstrated that the exciting electric field can be reduced by an order of magnitude while the large deformations can still be achieved with suitably designed heterogeneous actuators.<sup>[247]</sup>

The developments in micro-electromechanical systems and biomedical devices have raised more requirements for actuators, which need to be miniaturized, flexible, or biocompatible. The strategies used in the movements or deformations of living organisms fascinate scientists and biomimicking is regarded as a significant approach to designing high performance actuators. Many interesting work have been reported in this area, for example, the aforementioned hydrogel based actuating systems, in which the inhomogeneous structures play a key role. Compared to traditional actuators usually made of metal and ceramics, the biomimetic “soft” actuators prevail due to their flexibility, large deformation, and stimuli-responsiveness. However, there is still no actuating system with performance close to muscles that are both strong and fast. Soft actuators with enhanced mechanical strength and response rate, while the versatile mobility of which is simultaneously kept, will be desired in practical applications.

#### 4.4. Self-Healing Materials Based on Microvascular Networks

Long term stability is much desirable for the practical application of materials. Micro-cracks formed in bulk during use can expand gradually and finally lead to total failure of the materials. Hence, the ability of self-mending immediately when ruptures occur, just as living organisms possess, has been long pursued.

Self-healing ability can be defined as the power to repair or restore the mechanical strength or other properties such as conductivity<sup>[248]</sup> and transparency<sup>[249]</sup> spontaneously. Stimuli that trigger this process are usually the damages themselves or other ones such as heat, light, electricity and so on. Mechanical resilience, speed of response and period of validity are the dominating criteria for the evaluation of healing capacity.

Using encapsulated healing agents buried in bulk materials is the most traditional method to realize the self-repair function. However, capsule-based self-healing materials will not be discussed here since comprehensive reviews covering this strategy have existed.<sup>[250,251]</sup> The main focus of this part summarized the progress in the bio-inspired strategy using the 3D microvascular networks.

Our epiderm and bones can be automatically repaired with the help of blood vessels after injuries, as shown in Figure 14a. Although these biological processes take time and can be more complex than we could imagine, they really give us some enlightenments about how to construct a self-healing system. Synthetic microvascular network (Figure 14b) is such a product that mimics the healing system in living organisms. Breakage of these vasculatures at the crack plane results in the leakage and transportation of active agents in these channels, after which the self-repair takes place. Unlike using microcapsule-based

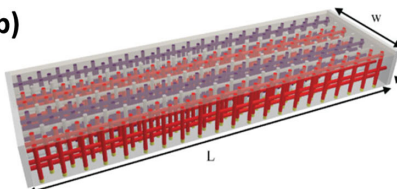
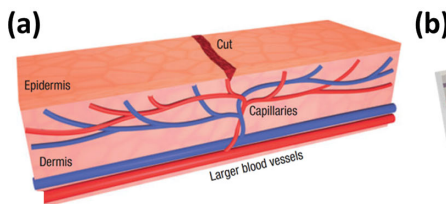


**Figure 14.** Schematic demonstration of (a) how human epidermis is healed with the help of blood vessels. Reproduced with permission.<sup>[252]</sup> Copyright 2007, Nature Publishing Group. (b) The dual microvascular networks used for self-healing.<sup>[254]</sup>

system, this strategy allows repeated healing and the employment of new healing agents.<sup>[252]</sup>

Sottos et al.<sup>[252]</sup> placed epoxy coating containing Grubb's catalyst on a ductile three-dimensional vascular substrate in which dicyclopentadiene monomer was stored. Ring-opening metathesis polymerization was automatically conducted after damage occurred, and repeated healing up to seven times could be achieved with a healing efficiency of up to 70%. Their further studies indicated that using dual microvascular networks to circulate epoxy resin and its hardener, respectively, will greatly improve the healing cycles and efficiencies, compared with simply holding the healing agents statically.<sup>[253,254]</sup> They also introduced the third interpenetrating network in which temperature-controlled fluid was circulated.<sup>[255]</sup> Healing process was accelerated when temperature was increased from 30 to 70 °C, and a rise in heal stress was observed in the meantime. The same group proved the feasibility of self-healing in bulk materials utilizing the multi-vascular networks by planting dual microvascular networks into epoxy resin, and healing efficiencies exceeding 40% in multiple healing processes were achieved and maintained until the networks were blocked.<sup>[256]</sup> Similarly, Trask et al.<sup>[257]</sup> applied vascular system in fiber reinforced composites laminate, and healing efficiency above 90% was obtained in a single healing process.

The key point of using microvascular system lies in the sufficiently mixing of the active agents in the crack planes.<sup>[254]</sup> However, limited by the slow diffusion of these healing chemicals and the high viscosity of the fluids adopted, fractures can hardly be totally wetted, thus leading to imperfect repair. In addition, the flow and mixing of these active agents can be easily blocked by previous healings. It should also be noted that the complexity and the cost of building such a 3D network in bulk materials can be very high, which is the weakness of this blood-vessel-inspired healing tactic. However, vascular based healing strategy is still very promising due to their extraordinary repeatable healing ability compared with other techniques.

## 5. Summary and Outlook

The idea of the preparation of manmade materials following the design principle of nature had been appeared occasionally in history, and has become more and more popular in the material research nowadays, and definitely this methodology will continue to play a key role in exploring new materials in the future. Although successful and fruitful results have been obtained in various fields, the biomimicry is still far from mature.

Firstly, there are still plenty of natural prototypes to be explored. For instance, superhydrophobic surfaces have been extensively studied since the lotus leaf effect was uncovered by Barthlott in 1997.<sup>[258]</sup> The occurrence of a composite solid-water-air interface between the surface and water, also named as Cassie state, is the key to realize self-cleaning, drag reducing, antifouling functions. Thousands of research papers have been published based on the combination of surface roughness and low surface energy to prepare lotus-leaf-like surfaces. However, the durability of superhydrophobicity is always poor, and the surface roughness generally conflicts with the surface transparency.

Recently, inspired by the *Nepenthes* pitcher plant, Aizenberg and coworkers fabricated slippery liquid-infused porous surface (SLIPS).<sup>[259]</sup> Unlike the common lotus-leaf-like surfaces on which air is trapped by the surface roughness, the pores of the SLIPS can be infused by special liquids to form a solid-water-liquid interface between the SLIPS and water. Excellent repellence to almost all kinds of liquids, and antifouling, anti-icing and anti-frost functions with high durability, transparency and even self-healing property have been realized on SLIPS,<sup>[260–263]</sup> demonstrating that better solutions enlightened by nature can always be found to solve the practical problems in the existing biomimicking systems.

Secondly, biomaterials are always self-organized using simple building blocks under mild conditions. The sophisticated hierarchical structures of biomaterials, however, have never been exactly copied by using modern technologies. Therefore, precisely controlling the structural formation in scales of centimeter, micrometer, and nanometer is still a great challenge. Given that the manmade building blocks to mimic the biomaterials are abundant and have superior properties than their natural counterparts, it is expectable to get bioinspired manmade materials with similar or even better performance with less comparable structure. This is especially important when the target materials are to be used in harsh working circumstances that are never faced by the natural prototypes.

Finally, most of the biomaterials are stimuli responsive, self-adaptive, and capable of self-healing by metabolism or other biological process. On the contrary, the bioinspired materials will generally lose their function once the structure was destroyed. Thus understanding and manipulating the dynamic and nanoscale molecular mechanisms of natural systems, replicating the adaptation and self-healing ability of biomaterials in bioinspired materials are important for future studies.

## Acknowledgements

The authors thank the financial support from (2014CB643600, 2012AA03A601) and NSFC (U1134105, 51373185, 51173194, 21210001).

Received: April 15, 2014

Revised: July 11, 2014

Published online: September 11, 2014

- [1] R. V. Lewis, *Chem. Rev.* **2006**, *106*, 3762.
- [2] M. E. McConney, K. D. Anderson, L. L. Brott, R. R. Naik, V. V. Tsukruk, *Adv. Funct. Mater.* **2009**, *19*, 2527.
- [3] E. S. Lintz, T. R. Scheibel, *Adv. Funct. Mater.* **2013**, *23*, 4467.
- [4] T. Bahners, U. Schlosser, R. Gutmann, E. Schollmeyer, *Sol. Energy Mater. Sol. Cells.* **2008**, *92*, 1661.
- [5] H. Tributsch, H. Goslawsky, U. Kuppers, H. Wetzel, *Sol. Energy Mater.* **1990**, *21*, 219.
- [6] F. Li, Y. Song, in *Nanofibers*, Vol. 22 (Eds: A. Kumar), INTECH, Croatia, **2010**, pp. 438.
- [7] F. T. Malik, R. M. Clement, D. T. Gethin, W. Krawszik, A. R. Parker, *Bioinspir. Biomim.* **2014**, *9*, 031002.
- [8] M. Liu, Y. Zheng, J. Zhai, L. Jiang, *Acc. Chem. Res.* **2010**, *43*, 368.
- [9] S. Nishimoto, B. Bhushan, *Rsc Advances* **2013**, *3*, 671.
- [10] A. Saito, *Sci. Technol. Adv. Mater.* **2011**, *12*, 064709.
- [11] D. Sameoto, C. Menon, *Smart Mater. Struct.* **2010**, *19*, 103001.
- [12] E. Ueda, P. A. Levkin, *Adv. Mater.* **2013**, *25*, 1234.
- [13] K. Tai, M. Dao, S. Suresh, A. Palazoglu, C. Ortiz, *Nat. Mater.* **2007**, *6*, 454.
- [14] Z. Tang, N. A. Kotov, S. Magonov, B. Ozturk, *Nat. Mater.* **2003**, *2*, 413.
- [15] B. Pokroy, V. Demensky, E. Zolotoyabko, *Adv. Funct. Mater.* **2009**, *19*, 1054.
- [16] B. J. Bruet, J. Song, M. C. Boyce, C. Ortiz, *Nat. Mater.* **2008**, *7*, 748.
- [17] W. Yang, I. H. Chen, B. Gludovatz, E. A. Zimmermann, R. O. Ritchie, M. A. Meyers, *Adv. Mater.* **2013**, *25*, 31.
- [18] S. F. Fischer, M. Thielen, R. R. Loprang, R. Seidel, C. Fleck, T. Speck, A. Bührig-Polaczek, *Adv. Eng. Mater.* **2010**, *12*, B658.
- [19] J. P. O'Brien, S. R. Fahnestock, Y. Termonia, K. C. H. Gardner, *Adv. Mater.* **1998**, *10*, 1185.
- [20] D. Porter, F. Vollrath, *Adv. Mater.* **2009**, *21*, 487.
- [21] I. Agnarsson, A. Dhinojwala, V. Sahni, T. A. Blackledge, *J. Exp. Biol.* **2009**, *212*, 1989.
- [22] B. An, J. E. Jenkins, S. Sampath, G. P. Holland, M. Hinman, J. L. Yarger, R. Lewis, *Biomacromolecules* **2012**, *13*, 3938.
- [23] Y. Hsia, E. Gnesa, R. Pacheco, K. Kohler, F. Jeffery, C. Vierra, *J. Vis. Exp.* **2012**, e4191.
- [24] O. Shchepelina, I. Drachuk, M. K. Gupta, J. Lin, V. V. Tsukruk, *Adv. Mater.* **2011**, *23*, 4655.
- [25] C. Ye, O. Shchepelina, R. Calabrese, I. Drachuk, D. L. Kaplan, V. V. Tsukruk, *Biomacromolecules* **2011**, *12*, 4319.
- [26] M. Heim, D. Keerl, T. Scheibel, *Angew. Chem. Int. Ed.* **2009**, *48*, 3584.
- [27] Z. Qin, M. J. Buehler, *Nat. Mater.* **2013**, *12*, 185.
- [28] Y. Zheng, H. Bai, Z. Huang, X. Tian, F. Nie, Y. Zhao, J. Zhai, L. Jiang, *Nature* **2010**, *463*, 640–643.
- [29] H. Bai, X. Tian, Y. Zheng, J. Ju, Y. Zhao, L. Jiang, *Adv. Mater.* **2010**, *22*, 5521.
- [30] H. Bai, R. Sun, J. Ju, X. Yao, Y. Zheng, L. Jiang, *Small* **2011**, *7*, 3429.
- [31] H. Bai, J. Ju, Y. Zheng, L. Jiang, *Adv. Mater.* **2012**, *24*, 2786.
- [32] T. Stegmaier, M. Linke, H. Planck, *Philos. Trans. R. Soc. A* **2009**, *367*, 1749.
- [33] Y. Zhao, X. Cao, L. Jiang, *J. Am. Chem. Soc.* **2007**, *129*, 764.
- [34] H. Xiang, Y. Long, X. Yu, X. Zhang, N. Zhao, J. Xu, *CrystEngComm* **2011**, *13*, 4856.
- [35] X. Zhang, C. Duan, N. Zhao, H. Xiao, M. Shi, X. Zhang, J. Xu, *Chin. J. Polym. Sci.* **2010**, *28*, 841.
- [36] H. Xiang, D. Wang, H. Liu, N. Zhao, J. Xu, *Chin. J. Polym. Sci.* **2013**, *31*, 521.
- [37] H. Chen, F. Rao, X. Shang, D. Zhang, I. Hagiwara, *J. Bionic Eng.* **2013**, *10*, 341.
- [38] J. Ju, H. Bai, Y. Zheng, T. Zhao, R. Fang, L. Jiang, *Nat. Commun.* **2012**, *3*, 1247.
- [39] K. Li, J. Ju, Z. Xue, J. Ma, L. Feng, S. Gao, L. Jiang, *Nat. Commun.* **2013**, *4*, 2276.
- [40] P. Qiu, C. Mao, *ACS Nano* **2010**, *4*, 1573.
- [41] G. Lin, Y. Tsai, H. Lin, C. Tang, C. Lin, *Langmuir* **2007**, *23*, 4115.
- [42] a) S. Kinoshita, S. Yoshioka, J. Miyazaki, *Rep. Prog. Phys.* **2008**, *71*, 076401; b) P. Vukusic, J. R. Sambles, *Nature* **2003**, *424*, 82; c) P. Vukusic, J. R. Sambles, C. R. Lawrence, *Nature* **2000**, *404*, 457.
- [43] V. Saranathan, C. O. Osuji, S. G. J. Mochrie, H. Noh, S. Narayanan, A. Sandy, E. R. Dufresne, R. O. Prum, *Proc. Natl. Acad. Sci. USA* **2010**, *107*, 11676.
- [44] R. H. Siddique, S. Diewald, J. Leuthold, H. Hölscher, *Opt. Express* **2013**, *21*, 14351.
- [45] K. Chung, S. Yu, C.-J. Heo, J. W. Shim, S.-M. Yang, M. G. Han, H.-S. Lee, Y. Jin, S. Y. Lee, N. Park, J. H. Shin, *Adv. Mater.* **2012**, *24*, 2375.
- [46] W. Zhang, D. Zhang, W. Chen, J. Gu, Q. Liu, S. Zhu, H. Su, C. Feng, W. J. Moon, *Int. J. Precis. Eng. Man.* **2012**, *13*, 1647.
- [47] S. Kang, T. Tai, T. Fang, *Curr. Appl. Phys.* **2010**, *10*, 625.
- [48] H. Yin, B. Dong, X. Liu, T. Zhan, L. Shi, J. Zi, E. Yablonovitch, *Proc. Natl. Acad. Sci. USA* **2012**, *109*, 10798.
- [49] S. N. Fernandes, Y. Geng, S. Vignolini, B. J. Glover, A. C. Trindade, J. P. Canejo, P. L. Almeida, P. Brogueira, M. H. Godinho, *Macromol. Chem. Phys.* **2013**, *214*, 25.
- [50] K. R. Thomas, M. Kolle, H. M. Whitney, B. J. Glover, U. Steiner, *J. R. Soc. Interface* **2010**, *7*, 1699.
- [51] S. Vignolini, P. J. Rudall, A. V. Rowland, A. Reed, E. Moyroud, R. B. Faden, J. J. Baumberg, B. J. Glover, U. Steiner, *Proc. Natl. Acad. Sci. USA* **2012**, *109*, 15712.
- [52] E. Shevtsova, C. Hansson, D. H. Janzen, J. Kjærandsen, *Proc. Natl. Acad. Sci. USA* **2011**, *108*, 668.
- [53] M. Riou, J. P. Christidès, *J. Chem. Ecol.* **2010**, *46*, 412.
- [54] M. Stevens, C. Rong, P. A. Todd, *Biol. J. Linn. Soci.* **2013**, *109*, 257.
- [55] J. H. Burroughes, C. A. Jones, R. H. Friend, *Synth. Met.* **1989**, *28*, C735.
- [56] M. A. Invernale, Y. Ding, D. M. D. Mamangun, M. S. Yavuz, G. A. Sotzing, *Adv. Mater.* **2010**, *22*, 1379.
- [57] H. Shin, Y. Kim, T. Bhuvana, J. Lee, X. Yang, C. Park, E. Kim, *ACS Appl. Mater. Interfaces* **2012**, *4*, 185.
- [58] J. Kim, J. You, B. Kim, T. Park, E. Kim, *Adv. Mater.* **2011**, *23*, 4168.
- [59] A. L. Dyer, E. J. Thompson, J. R. Reynolds, *ACS Appl. Mater. Interfaces* **2011**, *3*, 1787.
- [60] S. V. Vasilyeva, P. M. Beaujuge, Sh. J. Wang, J. E. Babiarz, V. W. Ballarotto, J. R. Reynolds, *ACS Appl. Mater. Interfaces* **2011**, *3*, 1022.
- [61] C. Chen, *J. Nanomater.* **2013**, *2013*, 785023.
- [62] C. Costa, C. Pinheiro, I. Henrique, C. A. T. Laia, *ACS Appl. Mater. Interfaces* **2012**, *4*, 1330.
- [63] S. Araki, K. Nakamura, K. Kobayashi, A. Tsuboi, N. Kobayashi, *Adv. Mater.* **2012**, *24*, OP122.
- [64] A. Tsuboi, K. Nakamura, N. Kobayashi, *Adv. Mater.* **2013**, *25*, 3197.
- [65] M. A. Invernale, Y. Ding, G. A. Sotzing, *ACS Appl. Mater. Interfaces* **2010**, *2*, 296.
- [66] T. Bhuvana, B. Kim, X. Yang, H. Shin, E. Kim, *Angew. Chem. Int. Ed.* **2013**, *52*, 1180.
- [67] K. Ueno, J. Sakamoto, Y. Takeoka, M. Watanabe, *J. Mater. Chem.* **2009**, *19*, 4778.
- [68] M. G. Han, C. G. Shin, S. Jeon, H. S. Shim, C. J. Heo, H. Jin, J. W. Kim, S. Y. Lee, *Adv. Mater.* **2012**, *24*, 6438.
- [69] J. Zhang, L. Wang, J. Luo, A. Tikhonov, N. Kornienko, S. A. Asher, *J. Am. Chem. Soc.* **2011**, *133*, 9152.
- [70] C. Liu, G. Gao, Y. Zhang, L. Wang, J. Wang, Y. Song, *Macromol. Rapid Commun.* **2012**, *33*, 380.
- [71] Q. Yang, S. Zhu, W. Peng, C. Yin, W. Wang, J. Gu, W. Zhang, J. Ma, T. Deng, C. Feng, D. Zhang, *ACS Nano* **2013**, *7*, 4911.
- [72] W. Hong, H. Li, X. Hu, B. Zhao, F. Zhang, D. Zhang, *Chem. Commun.* **2012**, *48*, 4609.

- [73] C. Fenzl, S. Wilhelm, T. Hirsch, O. S. Wolfbeis, *ACS Appl. Mater. Interfaces* **2013**, *5*, 173.
- [74] Y. Huang, F. Li, M. Qin, L. Jiang, Y. Song, *Angew. Chem. Int. Ed.* **2013**, *125*, 7437.
- [75] L. Jin, Y. Zhao, X. Liu, Y. Wang, B. Ye, Z. Y. Xie, Z. Gu, *Soft Matter* **2012**, *8*, 4911.
- [76] O. B. Ayyub, M. B. Ibrahim, R. M. Briber, P. Kofinas, *Biosens. Bioelectron.* **2013**, *46*, 124.
- [77] M. M. Hawkeye, M. J. Brett, *Adv. Funct. Mater.* **2011**, *21*, 3652.
- [78] L. Zulian, E. Emiliani, G. Scavia, C. Botta, M. Colombo, S. Destri, *ACS Appl. Mater. Interfaces* **2012**, *4*, 6071.
- [79] H. Hu, Q. Chen, K. Cheng, J. Tang, *J. Mater. Chem.* **2012**, *22*, 1021.
- [80] N. Kumano, T. Seki, M. Ishii, H. Nakamura, Y. Takeoka, *Angew. Chem. Int. Ed.* **2011**, *50*, 4012.
- [81] M. Chen, L. Zhou, Y. Guan, Y. Zhang, *Angew. Chem. Int. Ed.* **2013**, *125*, 10145.
- [82] K. Matsubara, M. Watanabe, Y. Takeoka, *Angew. Chem. Int. Ed.* **2007**, *46*, 1688.
- [83] C. G. Schäfer, M. Gallei, J. T. Zahn, J. Engelhardt, G. P. Hellmann, M. Rehahn, *Chem. Mater.* **2013**, *25*, 2309.
- [84] H. Fudouzi, T. Sawada, *Langmuir* **2006**, *22*, 1365.
- [85] Y. Yue, M. A. Haque, T. Kurokawa, T. Nakajima, J. Gong, *Adv. Mater.* **2013**, *25*, 3106.
- [86] M. N. Lejars, A. Margaillan, C. Bressy, *Chem. Rev.* **2012**, *112*, 4347.
- [87] M. Salta, J. A. Wharton, P. Stoodley, S. P. Dennington, L. R. Goodes, S. Werwinski, U. Mart, R. J. K. Wood, K. R. Stokes, *Phil. Trans. R. Soc. A* **2010**, *368*, 4729.
- [88] D. M. Yebra, S. Kiil, K. Dam-Johansen, *Prog. Org. Coat.* **2004**, *50*, 75.
- [89] L. D. Chambers, K. R. Stokes, F. C. Walsh, R. J. Wood, *Surf. Coat. Technol.* **2006**, *20*, 3642.
- [90] I. Omae, *Appl. Organomet. Chem.* **2003**, *17*, 81.
- [91] I. Banerjee, R. C. Pangule, R. S. Kane, *Adv. Mater.* **2011**, *23*, 690.
- [92] A. J. Scardino, R. de Nys, *Biofouling* **2011**, *27*, 73.
- [93] E. Ralston, G. Swain, *Bioinspir. Biomim.* **2009**, *4*, 015007.
- [94] C. Baum, W. Meyer, R. Stelzer, L.-G. Fleischer, D. Siebers, *Mar. Biol.* **2002**, *140*, 653.
- [95] A. V. Bers, M. Wahl, *Biofouling* **2004**, *20*, 43.
- [96] L. Hoipkermeier-Wilson, J. F. Schumacher, M. L. Carman, A. L. Gibson, A. W. Feinberg, M. E. Callow, J. A. Finlay, J. A. Callow, A. B. Brennan, *Biofouling* **2004**, *20*, 53.
- [97] A. Scardino, R. De Nys, *Biofouling* **2004**, *20*, 249.
- [98] J. Guenther, R. De Nys, *Biofouling* **2007**, *23*, 419.
- [99] A. Scardino, R. De Nys, O. Ison, W. O'Connor, P. Steinberg, *Biofouling* **2003**, *19*, 221.
- [100] M. L. Carman, T. G. Estes, A. W. Feinberg, J. F. Schumacher, W. Wilkerson, L. H. Wilson, M. E. Callow, J. A. Callow, A. B. Brennan, *Biofouling* **2006**, *22*, 11.
- [101] L. H. Wilson, J. F. Schumacher, J. A. Finlay, R. Perry, M. E. Callow, J. A. Callow, A. B. Brennan, *Abstracts of Papers of the American Chemical Society* **2005**, *230*, U4292.
- [102] K. Efimenko, J. Finlay, M. E. Callow, J. A. Callow, J. Genzer, *ACS Appl. Mater. Interfaces* **2009**, *1*, 1031.
- [103] C. Baum, W. Meyer, D. Roessner, D. Siebers, L. G. Fleischer, *Comp. Biochem. Physiol., Part A: Mol. Integr. Physiol.* **2001**, *130*, 835.
- [104] C. J. Long, J. F. Schumacher, P. A. C. Robinson, J. A. Finlay, M. E. Callow, J. A. Callow, A. B. Brennan, *Biofouling* **2010**, *26*, 411.
- [105] X. Cao, M. E. Pettitt, F. Wode, M. P. Arpa Sanctet, J. Fu, J. Ji, M. E. Callow, J. A. Callow, A. Rosenhahn, M. Grunze, *Adv. Funct. Mater.* **2010**, *20*, 1984.
- [106] C. M. Magin, C. J. Long, S. P. Cooper, L. K. Ista, G. P. López, A. B. Brennan, *Biofouling* **2010**, *26*, 719.
- [107] C. J. Long, J. A. Finlay, M. E. Callow, J. A. Callow, A. B. Brennan, *Biofouling* **2010**, *26*, 941.
- [108] K. C. Chaw, G. H. Dickinson, K. Y. Ang, J. Deng, W. R. Birch, *Biofouling* **2011**, *27*, 413.
- [109] P. Halder, M. Nasabi, F. J. T. Lopez, N. Jayasuriya, S. Bhattacharya, M. Deighton, A. Mitchell, M. A. Bhuiyan, *Biofouling* **2013**, *29*, 697.
- [110] J. Genzer, K. Efimenko, *Biofouling* **2006**, *22*, 339.
- [111] S. Krishnan, C. J. Weinman, C. K. Ober, *J. Mater. Chem.* **2008**, *18*, 3405.
- [112] H. Lee, S. M. Dellatore, W. M. Miller, P. B. Messersmith, *Science* **2007**, *318*, 426.
- [113] W. Yang, T. Cai, K. G. Neoh, E. T. Kang, G. H. Dickinson, S. L. M. Teo, D. Rittschof, *Langmuir* **2011**, *27*, 7065.
- [114] M. Zamfir, C. Rodriguez-Emmenegger, S. Bauer, L. Barner, A. Rosenhahn, C. Barner-Kowollik, *J. Mater. Chem. B* **2013**, *1*, 6027.
- [115] Y. Gong, L. P. Liu, P. B. Messersmith, *Macromol. Biosci.* **2012**, *12*, 979.
- [116] J. H. Cho, K. Shanmuganathan, C. J. Ellison, *ACS Appl. Mater. Interfaces* **2013**, *5*, 3794.
- [117] C. R. MatosPerez, J. J. Wilker, *Macromolecules* **2012**, *45*, 6634.
- [118] G. Li, H. Xue, C. Gao, F. Zhang, S. Jiang, *Macromolecules* **2010**, *43*, 14.
- [119] P. Bhadury, P. C. Wright, *Planta* **2004**, *219*, 561.
- [120] W. E. G. Mueller, X. Wang, P. Proksch, C. C. Perry, R. Osinga, J. Garderes, H. C. Schroeder, *Mar. Biotechnol.* **2013**, *15*, 375.
- [121] N. Aldred, I. Y. Phang, S. L. Conlan, A. S. Clare, G. J. Vancso, *Biofouling* **2008**, *24*, 97.
- [122] S. Dobretsov, H. Xiong, Y. Xu, L. A. Levin, P. Y. Qian, *Mar. Biotechnol.* **2007**, *9*, 388.
- [123] S. M. Olsen, J. B. Kristensen, B. S. Laursen, L. T. Pedersen, K. Dam-Johansen, S. Kiil, *Prog. Org. Coat.* **2010**, *68*, 248.
- [124] P. Shivapooja, Q. Wang, B. Orihuela, D. Rittschof, G. P. Lopez, X. Zhao, *Adv. Mater.* **2013**, *25*, 1430.
- [125] R. Brunner, O. Sandfuchs, C. Pacholski, C. Morhard, J. Spatz, *Laser Photonics Rev.* **2012**, *6*, 641.
- [126] K. Yu, T. Fan, S. Lou, D. Zhang, *Prog. Mater Sci.* **2013**, *58*, 825.
- [127] F. Liu, H. Yin, B. Dong, Y. Qing, L. Zhao, S. Meyer, X. Liu, J. Zi, B. Chen, *Phys. Rev. E* **2008**, *77*, 012901.
- [128] M. Kolle, P. M. Salgado-Cunha, M. R. Scherer, F. Huang, P. Vukusic, S. Mahajan, J. J. Baumberg, U. Steiner, *Nat. Nanotech.* **2010**, *5*, 511.
- [129] G. Zhang, J. Zhang, G. Xie, Z. Liu, H. Shao, *Small* **2006**, *2*, 1440.
- [130] J. Flicker, W. J. Ready, *Prog. Photovolt: Res. Appl.* **2014**, *22*, 634.
- [131] S. M. Luke, B. T. Hallam, P. Vukusic, *Appl. Opt.* **2010**, *49*, 4246.
- [132] J. H. Kim, J. H. Moon, S. Y. Lee, J. Park, *Appl. Phys. Lett.* **2010**, *97*, 103701.
- [133] Y. Li, J. Zhang, B. Yang, *Nano Today* **2010**, *5*, 117.
- [134] J. A. Hiller, J. D. Mendelsohn, M. F. Rubner, *Nat. Mater.* **2002**, *1*, 59.
- [135] K. Forberich, G. Dennler, M. C. Scharber, K. Hingerl, T. Fromherz, C. J. Brabec, *Thin Solid Films* **2008**, *516*, 7167.
- [136] X. Lu, Z. Wang, X. Yang, X. Xu, L. Zhang, N. Zhao, J. Xu, *Surf. Coat. Technol.* **2011**, *206*, 1490.
- [137] S. Wilson, M. Hutley, *J. Mod. Opt.* **1982**, *29*, 993.
- [138] D. Stavenga, S. Foletti, G. Palasantzas, K. Arikawa, *Proc. R. Soc. B* **2006**, *273*, 661.
- [139] D. Qi, N. Lu, H. Xu, B. Yang, C. Huang, M. Xu, L. Gao, Z. Wang, L. Chi, *Langmuir* **2009**, *25*, 7769.
- [140] Y. Huang, S. Chattopadhyay, Y. Jen, C. Peng, T. Liu, Y. K. Hsu, C. Pan, H. Lo, C. Hsu, Y. Chang, *Nat. Nanotech.* **2007**, *2*, 770.
- [141] Y. Li, J. Zhang, S. Zhu, H. Dong, F. Jia, Z. Wang, Z. Sun, L. Zhang, Y. Li, H. Li, W. Xu, B. Yang, *Adv. Mater.* **2009**, *21*, 4731.
- [142] Y. Kanamori, M. Sasaki, K. Hane, *Opt. Lett.* **1999**, *24*, 1422.
- [143] Y. Kanamori, K. Hane, H. Sai, H. Yugami, *Appl. Phys. Lett.* **2001**, *78*, 142.
- [144] H. Sai, H. Fujii, K. Arafune, Y. Ohshita, M. Yamaguchi, Y. Kanamori, H. Yugami, *Appl. Phys. Lett.* **2006**, *88*, 201116.

- [145] K. Hadobás, S. Kirsch, A. Carl, M. Acet, E. Wassermann, *Nanotechnology* **2000**, *11*, 161.
- [146] H. Deniz, T. Khudiyev, F. Buyukserin, M. Bayindir, *Appl. Phys. Lett.* **2011**, *99*, 183107.
- [147] Y. Li, J. Zhang, S. Zhu, H. Dong, Z. Wang, Z. Sun, J. Guo, B. Yang, *J. Mater. Chem.* **2009**, *19*, 1806.
- [148] D. H. Ko, J. R. Tumbleston, K. J. Henderson, L. E. Euliss, J. M. DeSimone, R. Lopez, E. T. Samulski, *Soft Matter* **2011**, *7*, 6404.
- [149] S. J. Choi, S. Y. Huh, *Macromol. Rapid Commun.* **2010**, *31*, 539.
- [150] L. Zhang, C. Lu, Y. Li, Z. Lin, Z. Wang, H. Dong, T. Wang, X. Zhang, X. Li, J. Zhang, B. Yang, *J. Colloid Interface Sci.* **2012**, *374*, 89.
- [151] S. M. Yang, S. G. Jang, D. G. Choi, S. Kim, H. K. Yu, *Small* **2006**, *2*, 458.
- [152] W. Shimizu, Y. Murakami, *ACS Appl. Mater. Interfaces* **2010**, *2*, 3128.
- [153] M. Faustini, L. Nicole, C. Boissiere, P. Innocenzi, C. Sanchez, D. Grossi, *Chem. Mater.* **2010**, *22*, 4406.
- [154] Y. Hoshikawa, H. Yabe, A. Nomura, T. Yamaki, A. Shimojima, T. Okubo, *Chem. Mater.* **2009**, *22*, 12.
- [155] X. Li, X. Du, J. He, *Langmuir* **2010**, *26*, 13528.
- [156] J. Moghal, J. Kobler, J. Sauer, J. Best, M. Gardener, A. A. Watt, G. Wakefield, *ACS Appl. Mater. Interfaces* **2012**, *4*, 854.
- [157] M. Manca, A. Cannavale, L. De Marco, A. S. Arico, R. Cingolani, G. Gigli, *Langmuir* **2009**, *25*, 6357.
- [158] L. Xu, J. He, *J. Mater. Chem. C* **2013**, *1*, 4655.
- [159] X. Li, J. He, *ACS Appl. Mater. Interfaces* **2012**, *4*, 2204.
- [160] X. Zhang, B. Xia, H. Ye, Y. Zhang, B. Xiao, L. Yan, H. Lv, B. Jiang, *J. Mater. Chem.* **2012**, *22*, 13132.
- [161] A. Yildirim, T. Khudiyev, B. Daglar, H. Budunoglu, A. K. Okyay, M. Bayindir, *ACS Appl. Mater. Interfaces* **2013**, *5*, 853.
- [162] J. Yun, T. S. Bae, J. D. Kwon, S. Lee, G. H. Lee, *Nanoscale* **2012**, *4*, 7221.
- [163] D. D. L. Chung, *J. Mater. Sci.* **2001**, *36*, 5733.
- [164] K. Urayama, T. Miki, T. Takigawa, S. Kohjiya, *Chem. Mater.* **2003**, *16*, 173.
- [165] H. Yamazaki, M. Takeda, Y. Kohno, H. Ando, K. Urayama, T. Takigawa, *Macromolecules* **2011**, *44*, 8829.
- [166] S. Suresh, *Science* **2001**, *292*, 2447.
- [167] P. Y. Chen, J. McKittrick, M. A. Meyers, *Prog. Mater Sci.* **2012**, *57*, 1492.
- [168] M. Thielen, T. Speck, R. Seidel, *J. Mater. Sci.* **2013**, *48*, 3469.
- [169] J. H. Waite, H. C. Lichtenegger, G. D. Stucky, P. Hansma, *Biochemistry* **2004**, *43*, 7653.
- [170] M. J. Harrington, A. Masic, N. Holten-Andersen, J. H. Waite, P. Fratzl, *Science* **2010**, *328*, 216.
- [171] K. U. Claussen, R. Giesa, T. Scheibel, H. W. Schmidt, *Macromol. Rapid Commun.* **2012**, *33*, 206.
- [172] X. Li, J. Xie, J. Lipner, X. Yuan, S. Thomopoulos, Y. Xia, *Nano Lett.* **2009**, *9*, 2763.
- [173] Y. Wang, Y. Wang, H. Zhang, L. Zhang, *Macromol. Rapid Commun.* **2006**, *27*, 1162.
- [174] C. Qin, W. Cai, J. Cai, D. Tang, J. Zhang, M. Qin, *Macromol. Chem. Phys.* **2004**, *85*, 402.
- [175] L. V. Karabanova, S. V. Mikhalkovsky, A. W. Lloyd, G. Boiteux, L. M. Sergeeva, T. I. Novikova, E. D. Lutsyk, S. Meikle, *J. Mater. Chem.* **2005**, *15*, 499.
- [176] J. H. Lee, J. P. Singer, E. L. Thomas, *Adv. Mater.* **2012**, *24*, 4782.
- [177] J. Aizenberg, J. C. Weaver, M. S. Thanawala, V. C. Sundar, D. E. Morse, P. Fratzl, *Science* **2005**, *309*, 275.
- [178] Y. H. Ha, R. A. Vaia, W. F. Lynn, J. P. Costantino, J. Shin, A. B. Smith, P. T. Matsudaira, E. L. Thomas, *Adv. Mater.* **2004**, *16*, 1091.
- [179] J. H. Jang, C. K. Ullal, T. Choi, M. C. Lemieux, V. V. Tsukruk, E. L. Thomas, *Adv. Mater.* **2006**, *18*, 2123.
- [180] M. Maldovan, C. K. Ullal, J. H. Jang, E. L. Thomas, *Adv. Mater.* **2007**, *19*, 3809.
- [181] L. Wang, M. C. Boyce, C. Wen, E. L. Thomas, *Adv. Funct. Mater.* **2009**, *19*, 1343.
- [182] J. H. Lee, L. Wang, S. Kooi, M. C. Boyce, E. L. Thomas, *Nano Lett.* **2010**, *10*, 2592.
- [183] L. Wang, M. C. Boyce, *Adv. Funct. Mater.* **2010**, *20*, 3025.
- [184] L. Wang, J. Lau, E. L. Thomas, M. C. Boyce, *Adv. Mater.* **2011**, *23*, 1524.
- [185] J. H. Lee, L. Wang, M. C. Boyce, E. L. Thomas, *Nano Lett.* **2012**, *12*, 4392.
- [186] N. Husing, U. Schubert, *Angew. Chem. Int. Ed.* **1998**, *37*, 23.
- [187] S. S. Kistler, *Nature* **1931**, *127*, 741.
- [188] J. P. Randall, M. A. B. Meador, S. C. Jana, *ACS Appl. Mater. Interfaces* **2011**, *3*, 613.
- [189] J. L. Gurav, I. K. Jung, H. H. Park, E. S. Kang, D. Y. Nadargi, *J. Nanomater.* **2010**, *2010*, 1.
- [190] J. Cai, S. Liu, J. Feng, S. Kimura, M. Wada, S. Kuga, L. Zhang, *Angew. Chem. Int. Ed.* **2012**, *51*, 2076.
- [191] Y. Duan, S. C. Jana, A. M. Reinsel, B. Lama, M. P. Espe, *Langmuir* **2012**, *28*, 15362.
- [192] Y. Duan, S. C. Jana, B. Lama, M. P. Espe, *Langmuir* **2013**, *29*, 6156.
- [193] X. Wang, S. C. Jana, *ACS Appl. Mater. Interfaces* **2013**, *5*, 6423.
- [194] X. Wang, S. C. Jana, *Langmuir* **2013**, *29*, 5589.
- [195] S. Nardeccchia, D. Carriazo, M. L. Ferrer, M. C. Gutierrez, F. del Monte, *Chem. Soc. Rev.* **2013**, *42*, 794.
- [196] H. Sun, Z. Xu, C. Gao, *Adv. Mater.* **2013**, *25*, 2554.
- [197] T. A. Schaeder, A. J. Jacobsen, A. Torrents, A. E. Sorensen, J. Lian, J. R. Greer, L. Valdevit, W. B. Carter, *Science* **2011**, *334*, 962.
- [198] Z. Wu, S. Yang, Y. Sun, K. Parvez, X. Feng, K. Müllen, *J. Am. Chem. Soc.* **2012**, *134*, 9082.
- [199] H. Hu, Z. Zhao, W. Wan, Y. Gogotsi, J. Qiu, *Adv. Mater.* **2013**, *25*, 2219.
- [200] A. Du, B. Zhou, Z. Zhang, J. Shen, *Materials* **2013**, *6*, 941.
- [201] A. S. Dorcheh, M. Abbasi, *J. Mater. Process. Technol.* **2008**, *199*, 10.
- [202] A. El Kadib, M. Bousmina, *Chem. Eur. J.* **2012**, *18*, 8264.
- [203] B. Ding, J. Cai, J. Huang, L. Zhang, Y. Chen, X. Shi, Y. Du, S. Kuga, *J. Mater. Chem.* **2012**, *22*, 5801.
- [204] X. Wu, T. Wen, H. Guo, S. Yang, X. Wang, A. Xu, *ACS Nano* **2013**, *7*, 3589.
- [205] Z. Wu, C. Li, H. Liang, J. Chen, S. Yu, *Angew. Chem. Int. Ed.* **2013**, *52*, 2925.
- [206] H. Bi, Z. Yin, X. Cao, X. Xie, C. Tan, X. Huang, B. Chen, F. Chen, Q. Yang, X. Bu, X. Lu, L. Sun, H. Zhang, *Adv. Mater.* **2013**, *25*, 5916.
- [207] L. Qiu, J. Liu, S. Chang, Y. Wu, D. Li, *Nat. Commun.* **2012**, *3*, 1241.
- [208] M. A. Meyers, P. Chen, A. Y. M. Lin, Y. Seki, *Prog. Mater Sci.* **2008**, *53*, 1.
- [209] Z. Xu, Y. Zhang, P. Li, C. Gao, *ACS Nano* **2012**, *6*, 7103.
- [210] D. Sanli, S. E. Bozbag, C. Erkey, *J. Mater. Sci.* **2012**, *47*, 2995.
- [211] L. Qian, H. Zhang, *J. Chem. Technol. Biotechnol.* **2011**, *86*, 172.
- [212] Z. Wang, Z. Dai, J. Wu, N. Zhao, J. Xu, *Adv. Mater.* **2013**, *25*, 4494.
- [213] Y. Osada, J. Gong, *Adv. Mater.* **1998**, *10*, 827.
- [214] Y. Qiu, K. Park, *Adv. Drug. Deliver. Rev.* **2001**, *53*, 321.
- [215] S. Chaterji, I. K. Kwon, K. Park, *Prog. Polym. Sci.* **2007**, *32*, 1083.
- [216] P. Calvert, *MRS Bull.* **2008**, *33*, 207.
- [217] G. Gerald, K. F. Arndt, *Hydrogel Sensors and Actuators*, Springer, Berlin **2009**.
- [218] L. Dong, A. K. Agarwal, D. J. Beebe, H. Jiang, *Nature* **2006**, *442*, 551.
- [219] L. Dong, A. K. Agarwal, D. J. Beebe, H. Jiang, *Adv. Mater.* **2007**, *19*, 401.
- [220] A. Sidorenko, T. Krupenkin, A. Taylor, P. Fratzl, J. Aizenberg, *Science* **2007**, *315*, 487.

- [221] A. Sidorenko, T. Krupenkin, J. Aizenberg, *J. Mater. Chem.* **2008**, *18*, 3841.
- [222] P. Kim, L. D. Zarzar, X. Zhao, A. Sidorenko, J. Aizenberg, *Soft Matter* **2010**, *6*, 750.
- [223] X. He, M. Aizenberg, O. Kuksenok, L. D. Zarzar, A. Shastri, A. C. Balazs, J. Aizenberg, *Nature* **2012**, *487*, 214.
- [224] P. J. Glazer, J. Leuven, H. An, S. G. Lemay, E. Mendes, *Adv. Funct. Mater.* **2013**, *23*, 2964.
- [225] Y. Wang, X. Liu, X. Li, J. Wu, Y. Long, N. Zhao, J. Xu, *Langmuir* **2012**, *28*, 11276.
- [226] P. Fratzl, F. G. Barth, *Nature* **2009**, *462*, 442.
- [227] C. Dawson, J. F. V. Vincent, A. M. Rocca, *Nature* **1997**, *390*, 668.
- [228] J. W. C. Dunlop, R. Weinkamer, P. Fratzl, *Mater. Today* **2011**, *14*, 70.
- [229] Z. Hu, X. Zhang, Y. Li, *Science* **1995**, *269*, 525.
- [230] Z. Liu, P. Calvert, *Adv. Mater.* **2000**, *12*, 288.
- [231] P. D. Topham, J. R. Howse, C. J. Crook, S. P. Armes, R. A. L. Jones, A. J. Ryan, *Macromolecules* **2007**, *40*, 4393.
- [232] T. A. Asoh, M. Matsusaki, T. Kaneko, M. Akashi, *Adv. Mater.* **2008**, *20*, 2080.
- [233] I. Y. Konotop, I. R. Nasimova, M. V. Tamm, N. G. Rambidi, A. R. Khokhlov, *Soft Matter* **2010**, *6*, 1632.
- [234] E. Wang, M. S. Desai, S. W. Lee, *Nano Lett.* **2013**, *13*, 2826.
- [235] Y. Liu, M. Takafuji, H. Ihara, M. Zhu, M. Yang, K. Gu, W. Guo, *Soft Matter* **2012**, *8*, 3295.
- [236] S. Zakharchenko, N. Puretskiy, G. Stoychev, M. Stamm, L. Ionov, *Soft Matter* **2010**, *6*, 2633.
- [237] G. Stoychev, N. Puretskiy, L. Ionov, *Soft Matter* **2011**, *7*, 3277.
- [238] G. Stoychev, S. Turcaud, J. W. C. Dunlop, L. Ionov, *Adv. Funct. Mater.* **2013**, *23*, 2295.
- [239] F. Ilievski, A. D. Mazzeo, R. F. Shepherd, X. Chen, G. M. Whitesides, *Angew. Chem. Int. Ed.* **2011**, *50*, 1890.
- [240] R. F. Shepherd, F. Ilievski, W. Choi, S. A. Morin, A. A. Stokes, A. D. Mazzeo, X. Chen, M. Wang, G. M. Whitesides, *Proc. Natl. Acad. Sci. USA* **2011**, *108*, 20400.
- [241] R. V. Martinez, J. L. Branch, C. R. Fish, L. Jin, R. F. Shepherd, R. M. D. Nunes, Z. Suo, G. M. Whitesides, *Adv. Mater.* **2013**, *25*, 205.
- [242] F. Cheng, R. Yin, Y. Zhang, C. Yen, Y. Yu, *Soft Matter* **2010**, *6*, 3447.
- [243] R. R. Kohlmeyer, J. Chen, *Angew. Chem. Int. Ed.* **2013**, *52*, 9234.
- [244] R. Pelrine, R. Kornbluh, Q. Pei, J. Joseph, *Science* **2000**, *287*, 836.
- [245] P. Brochu, Q. Pei, *Macromol. Rapid Commun.* **2010**, *31*, 10.
- [246] F. Carpi, R. Kornbluh, P. S. Larsen, G. Alici, *Bioinspi. Biomim.* **2011**, *6*, 045006.
- [247] S. Rudykh, A. Lewinstein, G. Uner, G. de Botton, *Appl. Phys. Lett.* **2013**, *102*, 151905.
- [248] B. J. Blaiszik, S. L. B. Kramer, M. E. Grady, D. A. McIlroy, J. S. Moore, N. R. Sottos, S. R. White, *Adv. Mater.* **2012**, *24*, 398.
- [249] A. C. Jackson, J. A. Bartelt, P. V. Braun, *Adv. Funct. Mater.* **2011**, *21*, 4705.
- [250] T. Nesterova, K. D. Johansen, L. T. Pedersen, S. Kiil, *Prog. Org. Coat.* **2012**, *75*, 309.
- [251] D. G. Shchukin, *Polym. Chem.* **2013**, *4*, 4871.
- [252] K. S. Toohey, N. R. Sottos, J. A. Lewis, J. S. Moore, S. R. White, *Nat. Mater.* **2007**, *6*, 581.
- [253] C. J. Hansen, W. Wu, K. S. Toohey, N. R. Sottos, S. R. White, J. A. Lewis, *Adv. Mater.* **2009**, *21*, 4143.
- [254] K. S. Toohey, C. J. Hansen, J. A. Lewis, S. R. White, N. R. Sottos, *Adv. Funct. Mater.* **2009**, *19*, 1399.
- [255] C. J. Hansen, S. R. White, N. R. Sottos, J. A. Lewis, *Adv. Funct. Mater.* **2011**, *21*, 4320.
- [256] A. R. Hamilton, N. R. Sottos, S. R. White, *Adv. Mater.* **2010**, *22*, 5159.
- [257] C. J. Norris, G. J. Meadoway, M. J. O'Sullivan, I. P. Bond, R. S. Trask, *Adv. Funct. Mater.* **2011**, *21*, 3624.
- [258] W. Barthlott, C. Neinhuis, *Planta* **1997**, *202*, 1.
- [259] T.-S. Wong, S. H. Kang, S. K. Y. Tang, E. J. Smythe, B. D. Hatton, A. Grinthal, J. Aizenberg, *Nature* **2011**, *477*, 443.
- [260] N. Vogel, R. A. Belisle, B. Hatton, T.-S. Wong, J. Aizenberg, *Nat. Commun.* **2013**, *4*, 2176.
- [261] X. Yao, Y. Hu, A. Grinthal, T.-S. Wong, L. Mahadevan, J. Aizenberg, *Nat. Mater.* **2013**, *12*, 529.
- [262] P. Kim, T.-S. Wong, J. Alvarenga, M. J. Kreder, W. E. Adorno-Martinez, J. Aizenberg, *ACS Nano* **2012**, *6*, 6569.
- [263] A. K. Epstein, T.-S. Wong, R. A. Belisle, E. M. Boggs, J. Aizenberg, *Proc. Natl. Acad. Sci. USA* **2012**, *109*, 13182.